THE UNIVERSITY OF CHICAGO

PSEUDOSPECTRAL SAMPLING OF GAUSSIAN BASIS SETS AS A NEW AVENUE TO HIGH-DIMENSIONAL QUANTUM DYNAMICS

A DISSERTATION SUBMITTED TO
THE FACULTY OF THE DIVISION OF THE PHYSICAL SCIENCES
IN CANDIDACY FOR THE DEGREE OF
DOCTOR OF PHILOSOPHY

DEPARTMENT OF CHEMISTRY

BY
CHARLES HEAPS

CHICAGO, ILLINOIS
MARCH 2016

TABLE OF CONTENTS

LIST OF FIGURES

LIST OF TABLES

ABSTRACT

This thesis presents a novel approach to modeling quantum molecular dynamics (QMD). Theoretical approaches to QMD are essential to understanding and predicting chemical reactivity and spectroscopy. We implement a method based on a trajectory-guided basis set. In this case, the nuclei are propagated in time using classical mechanics. Each nuclear configuration corresponds to a basis function in the quantum mechanical expansion. Using the time-dependent configurations as a basis set, we are able to evolve in time using relatively little information at each time step. We use a basis set of moving frozen (time-independent width) Gaussian functions that are well-known to provide a simple and efficient basis set for nuclear dynamics. We introduce a new perspective to trajectory-guided Gaussian basis sets based on existing numerical methods. The distinction is based on the Galerkin and collocation methods. In the former, the basis set is tested using basis functions, projecting the solution onto the functional space of the problem and requiring integration over all space. In the collocation method, the Dirac delta function tests the basis set, projecting the solution onto discrete points in space. This effectively reduces the integral evaluation to function evaluation, a fundamental characteristic of pseudospectral methods. We adopt this idea for independent trajectory-guided Gaussian basis functions. We investigate a series of anharmonic vibrational models describing dynamics in up to six dimensions. The pseudospectral sampling is found to be as accurate as full integral evaluation, while the former method is fully general and integration is only possible on very particular model potential energy surfaces. Nonadiabatic dynamics are also investigated in models of photodissociation and collinear triatomic vibronic coupling. Using Ehrenfest trajectories to guide the basis set on multiple surfaces, we observe convergence to exact results using hundreds of basis functions. The pseudospectral sampling of Gaussian basis functions introduces a new and efficient means of calculating the underlying quantum mechanics associated with trajectory-guided basis sets. We also discuss the conceptual connections to the quantum trajectory method and the benefits of solving quantum mechanics on a discrete grid. We include a chapter studying the

strengths and weaknesses of the parametric two-electron reduced-density-matrix (p2-RDM) method for systems susceptible to delocalization error. Density matrix methods are known to overestimate the energetic effects of electron delocalization, including severe effects such as diatomic dissociation to fractionally charged atoms. We consider the role of delocalization error in p2-RDM and demonstrate that the p2-RDM is resistant to delocalization error in challenging cases.

ACKNOWLEDGMENTS

This thesis represents the culmination of my academic experience at The University of Chicago. The work would never have been possible without the professional and personal relationships I have had the pleasure of developing over the years. I would like to acknowledge the role these individuals have played in the journey that has led me here.

First, I would like to thank my advisor, David Mazziotti. None of this would have been possible without his help and support over the years. I still remember our meeting when David first handed me a paper on Bohmian mechanics and quantum molecular dynamics and how lost I felt. In hindsight, I am deeply indebted to David for the opportunity to explore a world of science I never expected to pursue in my PhD. I am thankful for his patience, countless stimulating conversations and independence granted to me, leading to the work in this thesis.

I also want to thank the past and present members of the Mazziotti group, including Jay Foley, Srikant Veeraraghavan, Andrew Sand, Erik Hoy, Nick Rubin, Romit Chakraborty, Andrew Valentine, Erica Sturm, Charles Forgy, Anthony Schlimgen, Manas Sajjan, Kade Head-Marsden and Ali Raeber. And, of course, the undergraduates including Luke Bertels, Claire Liu, Alison McManus and Lexie McIsaac. They have always been there for stimulating conversations, not necessarily work related, and made the Mazziotti group experience a real pleasure.

I would like to acknowledge some of my instructors and mentors in the past that led me to graduate school. The first being Mr. Deangelis, my AP Chem teacher in high school. The Washington and Lee chemistry department, particularly Profs. Steve Desjardins and Erich Uffelman were invaluable in cultivating my interest in chemistry as a whole and theoretical chemistry in particular.

I especially want to thank my family. They have been tremendously supportive through all of my experiences, including graduate school. I never would have made it here had it not been for them.

Finally, I would like to thank Clare, who has been unconditionally supportive of me throughout graduate school. She has been there for the best and worst of times and been there at my side when I needed someone the most.

CHAPTER 1

INTRODUCTION

Quantum molecular dynamics is the study of the time evolution of chemical systems where quantum mechanical effects are important. Examples of processes that require quantum mechanical treatment include vibrational dynamics, electron dynamics, and non-adiabatic dynamics, or processes characterized by a breakdown of the Born-Oppenheimer approximation. In these cases, quantum mechanical effects such as coherence and energy quantization must be included in the dynamics. This is in contrast to classical dynamics, where a molecule may readily be treated as a collection of point charges moving according to classical equations of motion. The time-dependence of the quantum mechanical system is governed by the Schrödinger equation, which states that the time-derivative of the wave function is given by the Hamiltonian operating on the wave function at the given time. While the solution (for time-independent Hamiltonians) of the differential equation may readily be written down using the separation of variables, numerical implementation of the solution is very difficult. Numerical methods have been adopted from many fields and developed uniquely for quantum mechanics to offer effectively numerically exact solutions to the differential equation.

Although numerically exact methods are attractive because of there very high accuracy, they are ill-suited for many chemical applications. They generally require significant a priori knowledge of the dynamics before beginning the simulation and they are computationally demanding. Consider a molecule with n atoms in cartesian coordinates, which has $3n$ degrees of freedom. If we treat each degree of freedom with r basis functions, the basis set size will be r^{3N}. The calculation would likely require a matrix diagonalization or, at best, a fast Fourier transform. These become computationally intractable for more than a handful of atoms.

Accurate quantum molecular dynamics also requires accurate potential energy surfaces. In practice, the potential energy surface for nuclear dynamics is often generated from electronic structure calculations. Highly accurate calculations are required to correctly predict

the dynamics. However, electronic structure calculations are also computationally demanding, particularly when strong electron correlation is present. Therefore, significant error, computational effort, or both are introduced by relying on electronic structure calculations. Meaningful progress towards large scale quantum molecular dynamics simulations requires developments in both areas, ideally as a joint effort.

In my dissertation, we focus on vibrational and nonadiabatic dynamics. In vibrational dynamics, we begin with a localized and quantized vibrational wave function for the molecule known as a wave packet. As the nuclei move in time, the wave function corresponding to nuclear vibrations will, of course, change. Observing the evolution of the vibrational wave function in time is a valuable asset for understanding chemical processes. We may use the propagation to calculate spectra and predict reaction probabilities in scattering processes.

Additionally, sometimes the dynamics involve more than one electronic potential energy surface. When multiple electronic surfaces are similar in energy, there is a non-negligible probability that the wave function may transition to a different electronic state, referred to as nonadiabatic dynamics. In particular, two surfaces nearly degenerate in energy may lead to an avoided crossing, a point in the potential energy surface that allows transition between two electronic states without emission of radiation. Nonadiabatic dynamics are essential in describing many important chemical phenomena including excited state dynamics following photo excitation where intersystem crossings may occur (vibrationally coupled transitions between electronic states of different spins) or radiationless relaxation to the ground state of the same spin state. Nonadiabatic effects are also important in electron transfer and play significant roles in biological processes and electrochemical reactions.

In this dissertation, we confront the issue of efficient high-dimensional quantum molecular dynamics. In particular, we explore the use of trajectory-guided Gaussian wave packets as a basis for time-dependent quantum mechanics. We also briefly investigate the performance of two-electron reduced-density-matrix (2-RDM) electronic structure methods. In this chapter, we introduce two topics fundamental to the dissertation. First, we introduce the collocation

and Galerkin methods, which build the numerical framework for our discussion of quantum molecular dynamics methods. Second, we introduce the Gaussian wave packet and the associated equations of motion in preparation for their use as a basis set in future chapters.

1.1 The Collocation and Galerkin Numerical Methods

In this section, we introduce two common numerical methods, the collocation and Galerkin methods. Although we are interested in the Schrödinger equation, the ideas presented here are applicable to differential equations in many fields. We introduce the test function and discuss the error associated with different numerical approximations in a finite basis.

We begin by writing the time-dependent Schrödinger equation (TDSE) as

$$\left\langle \chi(x,t) \left| i\hbar\frac{\partial}{\partial t} - \hat{H} \right| \Phi(x,t) \right\rangle = R, \tag{1.1}$$

where we have introduced the test functions $\langle\chi(x,t)|$, an approximate solution $|\Phi(x,t)\rangle$, and the residual, R. If $|\Phi(x,t)\rangle$ were the exact solution, the residual would be zero. However, in practice the approximate solution is always finite and error is introduced from the finite representation of a function formally defined in an infinite-dimensional Hilbert space.[1] We may write $|\Phi(x,t)\rangle$ as a linear combination of basis functions,

$$|\Psi(x,t)\rangle \approx |\Phi(x,t)\rangle = \sum_{i}^{N} c_i(t)\phi_i(x,t), \tag{1.2}$$

so that the wave function is described using the expansion coefficients $\{c(t)\}$ and basis functions $\{\phi(x,t)\}$.

The objective, of course, is to minimize the residual. For the purpose of this discussion, the basis functions are taken to be linearly independent, and located in the domain of interest. The test function, which defines the sampling of the approximate solution, remains to be specified. The collocation and Galerkin methods are conveniently introduced through the

choice of test function in the "method of mean weighted residuals."[2, 3]

The canonical choice in introductory quantum mechanics is to use the basis functions as the test functions. This is only one particular choice of test function and defines the Galerkin method. In time-independent quantum chemistry, the selection is motivated by the variational method. The objective is to minimize

$$E_0 = \frac{\langle \Phi(x) | \hat{H} | \Phi(x) \rangle}{\langle \Phi(x) | \Phi(x) \rangle}, \tag{1.3}$$

where we have multiplied through by the complex conjugate of the wave function to calculate the expectation value. The variational method is based on the linear variation of the energy in terms of the expansion coefficients c_i. Therefore, we differentiate with respect to the coefficients and set the N expressions equal to zero. The result is the familiar eigenvalue problem in time-independent problems. The result is the familiar eigenvalue problem in time-independent problems, $H\Phi = E\Phi$. However, the expression is also finite-basis matrix equation for a differential equation employing the Galerkin method.

When a suitable basis is selected for the problem, the Galerkin method can be expected to provide stable and accurate results. However, consider the expression for the Hamiltonian,

$$H = -\left\langle \phi(x,t) \left| \frac{\hbar^2}{2m} \nabla^2 \right| \Phi(x,t) \right\rangle + \langle \phi(x,t) | V(x) | \Phi(x,t) \rangle, \tag{1.4}$$

where ∇^2 denotes the Laplacian and $|\phi(x,t)\rangle$ denotes the vector of basis functions. This requires integration over all space. For the purpose of our discussion, we will focus on basis sets of Gaussian functions. Gaussian bases are ubiquitous in quantum mechanics; they are the de facto basis in electronic structure theory and used in dynamics methods, including the work in this dissertation. One attractive feature of Gaussians is that they are easily integrated over all space. This includes the kinetic energy operator, where the integrals include polynomial coordinate terms.

The potential energy is more complicated. In electronic structure theory, the only poten-

tial energy is from the Coulomb potential, which is also analytically integrable for Gaussian basis sets. In molecular dynamics, the potential may be of an arbitrary form or only known at discrete points from electronic structure. Many conditions exist in which the potential energy integral is no longer analytically solvable. We review common methods to approximate the integral in Chapter 2.5.

Alternatively, we may choose the test function to be Dirac delta functions,

$$|\chi(x,t)\rangle = |\delta(x - x_i)\rangle, \tag{1.5}$$

which is known as collocation and characteristic of pseudospectral methods. Many of the first successful methods applied to quantum dynamics employ collocation, including the Fourier method and the discrete variable representation.[4–6]. Selecting the Dirac delta function as the test function forces the residual to be zero at the point of the delta function. Evaluating the integrals is now reduced to function evaluation, leading to potential energy matrix elements of the form

$$V_{ij} = \int_{-\infty}^{\infty} \delta(x - x_i) V(x) \phi_j(x) dx = V(x_i)\phi_j(x_i). \tag{1.6}$$

Clearly, this is a considerable simplification over the Galerkin integral. For this reason, pseudospectral methods are often chosen for numerical applications. Despite their popularity and simplicity, pseudospectral sampling has not been employed with trajectory-guided basis sets. We investigate a pseudospectral Gaussian formulation for time-dependent quantum molecular dynamics in this dissertation.

1.2 Time-dependent Gaussian Wave Packets

A fundamental component of the quantum molecular dynamics methods discussed here is the Gaussian basis set. The Gaussian basis set is a collection of localized functions specified

by their phase space (position, momentum) centers in which the wave function is expanded.

The form of the Gaussian basis function used throughout the dissertation is given by

$$\phi_i(\mathbf{x};\alpha_i,\mathbf{x}_i(t),\mathbf{p}_i(t),\gamma_i(t)) = \exp(\gamma_i)\prod_{k=1}^{N_d}\exp(-\alpha_{i_k}(x-x_{i_k})^2 + ip_{i_k}(x-x_{i_k})). \tag{1.7}$$

We define the N_d-dimensional (ith) basis function as a product of one-dimensional Gaussians. The basis function is a function only of the coordinates, where the bold denotes a vector spanning the N_d dimensions. The function parametrically depends on the time-dependent phase space center $(\mathbf{x}_i(t),\mathbf{p}_i(t))$, the time-independent width α_i (frozen Gaussians), and $\gamma_i(t)$, which is complex, accounting for phase and normalization. The normalization constant is $\gamma_i(t=0) = \sum_k^{N_d}\frac{1}{4}\ln(\frac{2\alpha_{ik}}{\pi})$.

The equations of motion for the Gaussian basis function may be derived from an expansion of the potential energy.[7] For simplicity, we work with a one-dimensional Gaussian inserted into the time-dependent Schrödinger equation

$$i\frac{\partial\phi}{\partial t} = \left(-\frac{1}{2m}\frac{\partial^2}{\partial x^2} + V(x_t) + V_x(x-x_t) + \frac{1}{2}V_{xx}(x-x_t)^2\right)\phi, \tag{1.8}$$

where

$$V_x = \left.\frac{dV(x)}{dx}\right|_{x=x_t} \tag{1.9}$$

and the second order is expansion for potentials with no higher than quadratic terms in x. The explicit kinetic energy and time derivative (denoted by over dot) of the Gaussian wave packet are

$$\dot{\phi} = \left(-\dot{\alpha}_t(x-x_t)^2 + (2\alpha_t\dot{x}_t - \dot{p}_t)(x-x_t) + i\dot{\gamma}_t + p_t\dot{x}_t\right)\phi \tag{1.10}$$

$$-\frac{1}{2m}\frac{\partial^2\phi}{\partial x^2} = -\frac{1}{2m}\left[-2\alpha_t + (-2\alpha_t(x-x_t) + ip_t)^2\right]\phi \tag{1.11}$$

Equating powers of $(x - x_t)$, we obtain the equations of motion

$$\dot{x}_t = \frac{p_t}{m} \tag{1.12a}$$

$$\dot{p}_t = -\left.\frac{dV(x)}{dx}\right|_{x_t} \tag{1.12b}$$

$$\dot{\gamma}_t = -i\left(V(x_t) + [2\alpha_t - p_t^2]/2m\right). \tag{1.12c}$$

$$\dot{\alpha}_t = -\frac{2\alpha_t^2}{m} - \frac{V_{xx}}{2} \tag{1.12d}$$

The equations of motion for the phase space center are in fact Hamilton's equations of motion.

Notice that the exact equations of motion for a Gaussian in a harmonic potential require time-dependence of the width parameter (thawed Gaussians). Although this should provide a more accurate description of the dynamics, we adopt frozen Gaussians for two reasons. First, thawed Gaussians introduce numerical instabilities into the dynamics when they are used as a basis set. If the basis functions broaden excessively, linear dependence compromises the quality of the dynamics. Second, the equation of motion for the width parameter requires the second derivative of the potential energy. In on-the-fly dynamics, when the potential energy is calculated by electronic structure, second derivative calculations require significantly more computational time. Also, since the second derivative of a quadratic potential is a constant, there exists a width parameter for a Gaussian in a harmonic well that has a fixed width. A Gaussian with a fixed width in a harmonic well is known as a coherent state.[1]

1.3 References

[1] D. Tannor, *Introduction to Quantum Mechanics: A Time-dependent Perspective* (University Science Books, 2007), ISBN 9781891389238.

[2] B. Finlayson, *The Method of Weighted Residuals and Variational Principles: With Appli-*

cation in Fluid Mechanics, Heat and Mass Transfer, Educational Psychology (Academic Press, 1972), ISBN 9780122570506.

[3] J. Boyd, *Chebyshev and Fourier Spectral Methods: Second Revised Edition*, Dover Books on Mathematics (Dover Publications, 2001), ISBN 9780486411835.

[4] M. D. Feit, J. Fleck, J. A., and A. Steiger, J. Comput. Phys. **47**, 412 (1982).

[5] J. Lill, G. Parker, and J. Light, Chem. Phys. Lett. **89**, 483 (1982).

[6] D. Kosloff and R. Kosloff, J. Comput. Phys. **52**, 35 (1983).

[7] E. J. Heller, J. Chem. Phys. **62**, 1544 (1975).

CHAPTER 2

TRAJECTORY-BASED NONADIABATIC MOLECULAR DYNAMICS

Trajectory-based methods have become some of the most popular approaches to studying quantum molecular dynamics. These range from independent classical trajectories to fully coupled quantum mechanical trajectories derived from the variational principle. In all cases, however, the advantages of a time-dependent basis set are exploited to study high-dimensional dynamics.

In this chapter, we focus on methods particularly important for the method development in this thesis. We focus on nonadiabatic, rather than adiabatic, methods because the latter may easily be deduced from the former in the limit of no coupling between potential energy surfaces. We begin with the full molecular Hamiltonian and review the the equations of motion for a general wave function spanning multiple electronic states, including the explicit form of coupling terms.

First, we discuss independent trajectory methods, including Ehrenfest dynamics and the fewest switches surface hopping algorithm. Although both methods have limitations because the trajectories are decoupled, they are the foundation of methods based on a basis set expansion of trajectories and are very useful in their own right. Next, we consider the *ab initio* multiple spawning (AIMS) algorithm. AIMS uses independent classical trajectories that form the basis for the solution of the time-dependent Schrödinger equation. Finally, we introduce nonadiabatic Bohmian dynamics. Bohmian dynamics offers a fully quantum mechanical dynamics method without a basis set expansion. We focus on the numerical implementation of the equations of motion and how we may adopt ideas from Bohmian mechanics to improve a basis set method for the time-dependent Schrödinger equation.

2.1 The Molecular Hamiltonian and Time-dependent Schrödinger Equation

We begin with the full nuclear and electronic time-dependent Schrödinger equation (TDSE),[1, 2]

$$i\frac{\partial}{\partial t}\Psi(r,x,t) = \hat{H}(r,x)\Psi(r,x,t), \tag{2.1}$$

and expand the total wave function using the Born-Huang expansion in the basis of orthonormal electronic states (I)[3],

$$\Psi(r,x,t) = \sum_{I}^{\infty} C^I(t)\Omega^I(r;x)\Phi^I(x,t). \tag{2.2}$$

where $\Omega(r;x)$ is electronic wave function, $\Phi(x,t)$ is the nuclear wave function, and r and x correspond to the electronic and nuclear coordinates, respectively.

The full electronic-nuclear molecular Hamiltonian for N_e electrons and N_n nuclei may be expressed as

$$\begin{aligned}\hat{H}(r,x) =& -\frac{1}{2}\sum_{\gamma}^{N_e}\nabla_{e,\gamma}^2 - \sum_{i}^{N_n}\frac{1}{2m_i}\nabla_{N,i}^2 + \sum_{\gamma<\alpha}\frac{1}{|r_\gamma - r_\alpha|} - \sum_{i,\gamma}\frac{Z_i}{|x_i - r_\gamma|} + \sum_{i<j}\frac{Z_i Z_j}{|x_i - x_j|} \\ =& \hat{T}_e(r) + \hat{T}_N(x) + \hat{V}_e(r) + \hat{V}_{Ne}(r,x) + \hat{V}_N(x) \\ =& -\sum_{i}^{N_n}\frac{1}{2m_i}\nabla_{N,i}^2 + \hat{H}_{\text{el}}(r;x)\end{aligned} \tag{2.3}$$

where Greek indices label electrons, Latin indices label nuclei, Z denotes nuclear charge, and $\{\nabla_e^2, \nabla_N^2\}$ are derivatives with respect to the electronic and nuclear coordinates, respectively. The third line reduces the Hamiltonian to the nuclear kinetic energy operator and the electronic energy.

The nuclear kinetic energy operator acting on the full wave function produces

$$T_N\{\Omega(r;x,t)\Phi(x,t)\} = -\sum_i^{N_n}\frac{1}{2m_i}\Big(\Omega(r;x,t)\nabla_i^2\Phi(x,t)+ \\ 2\nabla_i\Omega(r;x,t)\nabla_i\Phi(x,t) + \Phi(x,t)\nabla_i^2\Omega(r;x,t)\Big), \tag{2.4}$$

where the subscript has been dropped from ∇_N and all subsequent gradients are with respect to nuclear coordinates. In the Born-Oppenheimer approximation, the nuclear kinetic energy is neglected because of mass ratios. The ratio of T_e/T_N is proportional to the masses of the electrons and nuclei, which usually differ by orders of magnitude. The first term on the RHS Eq. (2.4) is the nuclear kinetic energy while the second and third terms account for coupling between the nuclear and electronic wave functions. In the second and third terms, there are derivatives of the *electronic* wave function with respect to the *nuclear* coordinates. In adiabatic dynamics, the second and third terms on the RHS are neglected.

Inserting the Born-Huang expansion into the molecular Hamiltonian and integrating over the electronic degrees of freedom produces

$$i\frac{\partial}{\partial t}\Phi^I(x,t) = \left[-\sum_i^{N_n}\frac{1}{2m_i}\nabla_i^2 + E_{\text{el}}^I\right]\Phi^I(x,t) \\ + \sum_J^{\infty} d^{IJ}(x) + g^{IJ}(x). \tag{2.5}$$

The terms in the summation account for coupling between multiple electronic states and the nuclei and electronic wave functions. The explicit form for the first and second derivative couplings, respectively, are

$$d^{IJ}(x) = \sum_i^{N_n}\frac{1}{m_i}\nabla_i\Phi^J(x)\int\Omega^I(r;x)\nabla_i\Omega^J(r;x)dr \tag{2.6}$$

$$g^{IJ}(x) = \Phi^J(x)\sum_i^{N_n}\frac{1}{2m_i}\int\Omega^I(r;x)\nabla_i^2\Omega^J(r;x)dr. \tag{2.7}$$

Since the gradient operator is anti-Hermitian, the first derivative coupling is zero for elements diagonal in the electronic state index $I = J$. Additionally, the first derivative coupling is a vector quantity and defined along each coordinate. The second derivative couplings, however, are present for both diagonal and off-diagonal indices.

In adiabatic dynamics, the terms g^{II} are neglected because of the slow motion of the nuclei. Including the diagonal second derivative coupling is a correction to Born-Oppenheimer dynamics but does not contribute to population exchange between potential energy surfaces. The second derivative couplings are generally neglected because of their small size and will be omitted in the presentation of numerical methods.[4] These coupling terms between potential energy surfaces are a purely quantum mechanical effect. Derivative couplings are responsible for population exchange observed when two or more adiabatic surfaces are not well separated energetically.

2.2 Adiabatic and Diabatic Representations

In this section, we briefly introduce a distinction between the adiabatic representation and the diabatic representation for nonadiabatic dynamics. Nonadiabatic dynamics refers to nuclear dynamics occurring on more than one potential energy surface. However, one may use either diabatic or adiabatic surfaces.

Adiabatic surfaces are eigenstates of the electronic Hamiltonian. The coupling between surfaces occurs through the nuclear kinetic energy operator. The adiabatic representation is convenient for molecular dynamics because electronic structure programs calculate adiabatic surfaces, allowing straightforward implementation with the equations of motion. However, the derivative coupling, given by Eq. (2.6), is often rapidly varying in the region of an avoided crossing, complicating numerical implementations.

A diabatic states is defined as an electronic state that does not change physical character as one moves along a reaction coordinates.[5] As a result, diabatic surfaces are smooth with respect to nuclear coordinates, which is highly desirable for both simulation and con-

ceptualization of reactions. Since the electronic state changes minimally with respect to nuclear coordinates, the derivative coupling is zero (or very small) for diabatic states and interstate coupling occurs through off-diagonal elements of the potential energy. Since the time-dependent Schrödinger equation is no longer represented in the adiabatic basis (basis of electronic eigenstates), the potential energy is not necessarily diagonal. Therefore, we introduce the off-diagonal potential energy $V^{IJ}(x)$ to the sum over J in Eq. (2.5). The potential energy now accounts for population exchange between states. While diabatic states are amenable to dynamics simulations, no rigorous transformation exists from adiabatic to diabatic surfaces. Nevertheless, considerable success has been realized in developing approximate transformations for dynamics.[6–15]

2.3 Ehrenfest Dynamics

Despite our emphasis on the Born-Huang expansion of the molecular wave function, we begin with a method based on a single (not a linear combination) wave function ansatz. Ehrenfest dynamics are particularly relevant because the potential energy defined by the Ehrenfest potential is used to propagate trajectories in later chapters. The underlying principle of Ehrenfest trajectories is to define a single, effective potential energy surface defined by the expectation value of the Hamiltonian.

The wave function in Ehrenfest dynamics is given as the single product,

$$\Psi(r,x,t) = \Omega(r,t)\Phi(x,t)\exp\left(i\int_{t_0}^{t} dt' E_{el}(t')\right), \tag{2.8}$$

where Ω is the electronic wave function, Φ is the nuclear wave function, and the phase factor is defined as

$$E_{el} = \int\int \Phi^*(x,t)\Omega^*(r,t)\hat{H}_{el}(r,x)\Phi(x,t)\Omega(r,t)drdx, \tag{2.9}$$

which satisfies the TDSE. After some algebra, [2, 16] we may write a system of mean-field

coupled equations

$$i\frac{\partial\Omega(r,t)}{\partial t} = -\frac{1}{2}\sum_{\gamma}\nabla_{\gamma}^{2}\Omega^{*}(r,t) + \left[\int \Phi(x,t)\hat{V}(r;x)\Phi(x,t)dx\right]\Omega(r,t) \tag{2.10}$$

$$i\frac{\partial\Phi(x,t)}{\partial t} = -\sum_{i}\frac{1}{2m_i}\nabla_{i}^{2}\Phi(x,t) + \left[\int \Omega^{*}(r,t)\hat{H}_{el}(r,x)\Omega(r,t)dr\right]\Phi(x,t). \tag{2.11}$$

Notice that the first terms on the RHS of Eqs. (2.10) and (2.11) are the kinetic energy for the electrons and nuclei respectively, and the second term defines an averaged potential energy dictating the dynamics.

The most important takeaway from these equations is that the potential energy surface guiding the nuclear wave function is defined by the quantum mechanical expectation value for the potential energy. In dynamics on multiple electronic surfaces, this means that the nuclei will be guided by an averaged potential energy surface. Although the simplicity of Ehrenfest trajectories is attractive, there is a qualitative failure in the methodology. Consider the molecular dynamics of two potential energy surfaces where the ground state is bound and the excited state is dissociative. As the dynamics evolve, population will be exchanged between the two states. If one tries to average the potential energy between a bound and dissociative state, you arrive at a potential energy that explains both channels poorly.

2.4 Fewest-Switches Surface-Hopping

The fewest-switches surface-hopping (FSSH) method of Tully, is likely the single most popular method for nonadiabatic dynamics.[16, 17] In, FSSH, independent trajectories representing classical, point-particle nuclei, are propagated classically on an adiabatic surface. In regions where nonadiabatic coupling, the quantum mechanical coupling is described using a stochastic, "hopping" prescription. The hopping overcomes the fundamental shortcoming of Ehrenfest dynamics. While the averaged potential may poorly describe the reaction channels, an FSSH trajectory always follows a single potential energy surface. If one runs

enough trajectories, the ensemble average should provide information on the final state of the quantum mechanical system.[18–25]

Although there are multiple ways to derive FSSH, we follow Refs. [2, 16, 17, 26], which begins with the Born-Huang expansion, and assumes that the nuclear wave function as a classical point particle,

$$\Phi(x,t) = \prod_i \delta(x_i - x_i(t)), \tag{2.12}$$

allowing us to write the wave function as

$$\Psi(r,x,t) = \sum_I^{\infty} C^I(t)\Omega^I(r;x), \tag{2.13}$$

where $C^I(t)$ is the nuclear amplitude on the Ith electronic state. Inserting the wave function expansion into the TDSE and integrating over the electronic coordinates, we can write

$$i\dot{C}^I = \sum_J C^J \left(V^{IJ}(x_i) - id^{IJ}(x_i)\right), \tag{2.14}$$

where the definition if the derivative coupling is given by Eq. (2.6).

The improvement in FSSH over Ehrenfest-type dynamics is in the definition of the trajectory associated with the wave function. Rather than evolving on an averaged surface, FSSH trajectories always follow classical equations of motion defined by a single potential energy surface. While the coefficients $\{C\}$ evolve in time, they do not directly determine the trajectory potential. Rather, trajectories evolve on a single surface and based on the coefficients have a probability of "hopping" to a different surface and continuing the dynamics on that surface. Tully prescribed a transition probability for the fewest switches defined as

$$\beta_{\text{hop}}^{I\to J} = -\sum_i \frac{2p_i}{m_i}\frac{\text{Re}(d_i^{IJ}(x)\sigma^{IJ})}{\sigma^{II}}dt, \tag{2.15}$$

where p_i is the momentum for the *i-th* degree of freedom, $\sigma^{IJ} = C^{I*}C^J$ are the electronic

density matrix elements and dt is the time step in the calculation. In the calculation, a random number ξ is generated between zero and one and if $\beta_{\text{hop}}^{I\to J} > \xi$, then the trajectory will move to surface J and become motion according to that potential energy. The momentum will usually be rescaled to preserve the total energy of the trajectory.

If we return to the case of a two-surface case describing a bound an dissociative state, we can see the advantage of FSSH. Since each trajectory follows a single surface, it will either remain bound or dissociate. Ideally, averaging over a sufficient number of trajectories, you can obtain state populations that account for different reaction channels. While FSSH has been tremendously successful, in part because of it's simplicity, there are some fundamental issues that limit the applicability of FSSH. First, the trajectories are independent, preventing any nonlocal (quantum) behavior between trajectories from being described in the nuclei. Additionally, the evolution of the nuclear probabilities by Eq. (2.14) does not properly describe decoherence between electronic states. The over coherence leads to spurious results for long-time dynamics, particularly when multiple passages through regions of derivative coupling occur.[23, 27, 28]

2.5 *ab initio* Multiple Spawning

We now turn to the *ab initio* multiple spawning (AIMS) algorithm of Martínez and coworkers.[29–39] AIMS overcomes the shortcomings of both Ehrenfest dynamics and FSSH, but at significant computational expense. In AIMS, the full Schrödinger is solved using a time-dependent basis set of Gaussians. As a result, a matrix equation of the form $Ax = b$ must be solved at each time step. While this is obviously more expensive than running independent trajectories, convergence is often realized using relatively few trajectories.

The AIMS method improves over other trajectory-guided basis set method by allowing the time-dependent basis set to grow over time. Similar to FSSH, each trajectory has probability amplitude on all surfaces, but the forces guiding the trajectory are determined by a single surface. When the wave packet encounters a region of coupling, populating other surfaces,

the method "spawns" basis functions on the other surfaces. The new basis function is guided by the forces of the newly populated surface. As a result, the method easily handles wave packet separation in circumstances such as the bound vs. dissociative case.

We review the AIMS method in this chapter as a prototypical Galerkin time-dependent Gaussian basis set method. [39–50] The spawning procedure has enabled unprecedented systems to be studied using Gaussian basis sets. However, the quantum mechanical matrix equations are similar, or identical, to other time-dependent basis set methods. In particular, all of these methods face the same challenges evaluating the potential energy integrals.

The quantum mechanical framework for AIMS is based on the time-dependent basis functions introduced in section 1.2 and the Galerkin formulation introduced in section 1.1. Within the Born-Huang expansion in Eq. (2.2), we may expand the nuclear wave function for a given electronic state in the basis of Gaussians

$$|\Phi^I(x,t)\rangle = \sum_i^N c_i(t)\phi_i(x,t), \tag{2.16}$$

The coefficients $C^I(t)$ define the probability of the nuclear wave packet on surface I while $c_i(t)$ are responsible for intra-surface coupling of the wave packet. For simplicity we may introduce a new coefficient, $D_i^I = C^I(t)c_i(t)$, which defines both the inter and intra-surface coupling. Since the basis is time-dependent, we write the TDSE as

$$i\frac{\partial}{\partial t}|\Phi^I(x,t)\rangle = i\sum_i^N \left(\phi_i(x,t)\frac{d}{dt}D_i^I(t) + D_i^I(t)\frac{\partial}{\partial t}\phi_i(x,t)\right) = \sum_i^N \hat{H}\phi_i(x,t). \tag{2.17}$$

Now, we select the basis function as the test function, as in the Galerkin method, and use the multi-state Hamiltonian given by Eq. (2.5). The final form of the TDSE becomes

$$\dot{\mathbf{D}}^I = i\mathbf{S}^{-1}\left(\mathbf{H}^{II} - i\dot{\mathbf{S}}\right)\mathbf{D}^I + \sum_{I\neq J}\mathbf{H}^{IJ}\mathbf{D}^J, \tag{2.18}$$

where $\mathbf{S}$ is the overlap matrix, $\mathbf{H}$ is the Hamiltonian and $\dot{\mathbf{S}}$ is the time-derivative of the overlap matrix. The inverse of the overlap matrix does not enter into the terms for $I \neq J$ because of the orthogonality of the electronic states. Examples of the matrix elements are

$$S_{ij} = \int_{-\infty}^{\infty} \phi_i^*(x,t)\phi_j(x,t)dx \tag{2.19}$$

$$\dot{S}_{ij} = \int_{-\infty}^{\infty} \phi_i^*(x,t)\frac{\partial}{\partial t}\phi_j(x,t)dx \tag{2.20}$$

$$H_{ij} = -\frac{1}{2m}\int_{-\infty}^{\infty} \phi_i^*(x,t)\frac{\partial^2}{\partial x^2}\phi_j(x,t)dx + \int_{-\infty}^{\infty} \phi_i^*(x,t)V(x)\phi_j(x,t)dx. \tag{2.21}$$

All of these integrals except for the second term on the RHS of Eq. (2.21) are easily solved analytically for Gaussian basis sets. We have omitted the inter-surface coupling terms, but they are evaluated similarly. Integrals involving the derivative coupling, $d^{IJ}(x)$ or the diabatic interstate coupling $V^{IJ}(x)$, are approximated in the same fashion as the potential energy integral in Eq. (2.21).

Since the potential energy integral is generally not analytically solvable approximations must be introduced. The approximation of potential energy integrals is critical for accurate time evolution and a principal interest of our research. Here, we present some of the most common approximations employed in both AIMS and other Gaussian-based methods. The problem of evaluating the potential energy integral stems directly from the implementation challenges of Galerkin methods discussed in Chapter 1.1. With the discussion of Galerkin and collocation methods in mind, we will pursue a collocation form of trajectory-based Gaussian dynamics.

When dynamics calculations are run using electronic structure calculations, the potential energy information is usually point wise, corresponding to distinct calculations, which requires an expression for the integral in terms of local quantities. This may be bypassed by fitting the potential energy surface to an analytical function, but fitting rapidly becomes difficult in higher dimensions. A natural choice to evaluate the integral is to evaluate the

potential energy using a Taylor series expansion around the point x_c,

$$V(x) = V(x_c) + \left.\frac{dV(x)}{dx}\right|_{x=x_c}(x - x_c) + \frac{1}{2!}\left.\frac{d^2V(x)}{dx^2}\right|_{x=x_c}(x - x_c)^2. \tag{2.22}$$

For diagonal elements, x_c is easily selected to be the center of the basis function. For off-diagonal elements, we can expand around the centroid of the basis functions and use only the zeroth order term,

$$V_{ij} = \langle\phi_i(x)|V(x)|\phi_j\rangle \approx \langle\phi_i|\phi_j\rangle V\left(\frac{\alpha_i x_i + \alpha_j x_j}{\alpha_i + \alpha_j}\right) = S_{ij}V(\tilde{x}), \tag{2.23}$$

where $\tilde{x}$ is the centroid of two basis functions. This approximation has been commonly used in AIMS and is called the saddle point approximation (SPA).[29, 31] The most significant problem with the SPA is that the off-diagonal elements require additional electronic structure calculations, scaling as $\mathcal{O}(N^2)$ with respect to basis set size. It would be much better if only the electronic structure required for the trajectories was used in calculating the matrix elements.

In order to produce an $\mathcal{O}(N)$ approximation, we average over expansions about each basis set center, known as the bra-ket averaged Taylor expansion (BAT). The explicit form for the matrix elements is

$$\begin{aligned} V_{ij} =& \langle\phi_i|V(x)|\phi_j\rangle \approx S_{ij}\left(\frac{V(x_i) + V(x_j)}{2}\right) \\ &+ \left(\frac{\langle\phi_i|(x - x_j)|\phi_j\rangle\nabla V(x_j) + \langle\phi_i|(x - x_i)|\phi_j\rangle\nabla V(x_i)}{2}\right). \end{aligned} \tag{2.24}$$

The difference between the SPA and BAT may be considered the difference between $V((i + j)/2)$ and $(V(i) + V(j))/2$. Fortunately, $V(i)$ and $V(j)$ are already required for the propagation of the classical trajectories, so the off-diagonal elements do not require additional electronic structure calculations in the BAT, unlike the SPA. The BAT is able to include first order terms since the gradients at the basis function centers are also required to propagate the

trajectories. This reduction in scaling can provide significant computational improvement when the evaluation of V is expensive, as in on-the-fly dynamics.

A final approximation that has been frequently used is the local harmonic approximation (LHA).[51] The LHA originated in early Gaussian work and is often quite accurate.[43, 52] Unfortunately, the LHA scales as $\mathcal{O}(N^2)$ *and* requires second derivatives of the potential energy surface. As a result, it is a very expensive approximation that is less suitable for on-the-fly dynamics.

2.6 Nonadiabatic Bohmian Dynamics

We conclude with Nonadiabatic Bohmian Dynamics (NABDY), a formally exact fully quantum mechanical formulation for nonadiabatic dynamics.[2, 26, 53] The equations of motion are determined by inserting the Bohmian, or polar, form of the wave function into the time-dependent Schrödinger equation. NABDY is a generalization of the quantum trajectory method (QTM), introduced by Lopreore and Wyatt in 1999.[54] Although the formally exact nature is attractive, implementation of NABDY is difficult because of numerical instabilities, limiting the applicability of the method to date.

The Bohmian wave function form is

$$\Phi^I(x,t) = A^I(x,t) \exp\left(iS^I(x,t)\right), \tag{2.25}$$

where $A^I(x,t)$ and $S^I(x,t)$ are the amplitude and phase of the nuclear wave function on surface I. The equations of motion are derived by directly inserting the wave function ansatz into Eq. (2.5). Separating the terms into real and imaginary parts, we obtain a

coupled set of differential equations,

$$\begin{aligned}\frac{dS^I(x,t)}{dt} =& \frac{1}{2m}(\nabla S^I(x,t))^2 - V^I(x) \\ &+ \frac{1}{2m}\frac{\nabla^2 A^I(x,t)}{A^I(x,t)} \\ &+ \sum_{J,I\neq J}\frac{1}{m}d^{IJ}(x)\frac{\nabla A^J(x,t)}{A^I(x,t)}\Re(\Xi^{IJ}) \\ &- \sum_{J,I\neq J}\frac{1}{m}d^{IJ}(x)\frac{A^J(x,t)}{A^I(x,t)}d^{IJ}(x)\nabla S^J(x,t)\Im(\Xi^{IJ})\end{aligned} \tag{2.26}$$

$$\begin{aligned}\frac{dA^I(x,t)}{dt} =& -\frac{1}{2m}A^I(x,t)\nabla^2 S^I(x,t) \\ &+ \sum_{J,I\neq J}\frac{1}{m}d^{IJ}(x)\nabla A^J(x,t)\Im(\Xi^{IJ}) \\ &- \sum_{J,I\neq J}\frac{1}{m}A^J(x,t)d^{IJ}(x)\nabla S^J(x,t)\Re(\Xi^{IJ}).\end{aligned} \tag{2.27}$$

We have neglected the second derivative coupling and used the relationship that $v = \nabla S^I(x,t)/m$, defining the momentum as the gradient of the phase of the wave function. In the original form, the equations of motion correspond to fixed points in space. However, we can transform from the Eulerian to the Lagrangian frame using

$$\frac{d}{dt} = \frac{\partial}{\partial t} + v\nabla. \tag{2.28}$$

Introducing the velocity allows the grid points to move in time along with the quantum mechanical probability, rather than exchanging probability between stationary points to evolve the system. The factor $\Xi^{IJ} = \exp(i[S^I(x,t) - S^J(x,t)])$ defines the phase relationship between the wave functions on different electronic surfaces. The third term of the RHS of Eq. 2.26 is known as the quantum potential. The amplitude, $A(x,t)$, is in the denominator and therefore the quantum potential becomes unstable at wave function nodes, or cases where the amplitude is very small.

The unique feature of Bohmian mechanics is that these equations may be solved without introducing a basis set. The problem is solved by discretizing the wave packet onto a grid of points, each of which has an amplitude and phase determined by the full wave function. Numerically, the problem is reduced to the evaluation of spatial derivatives of the amplitude and phase on a set of points, which becomes challenging for complicated dynamics.[54–60] The representation is sometimes called the hydrodynamic formulation of quantum mechanics and because of the similarities to fluid mechanics, the discrete points are called fluid elements.

Despite numerical challenges, the QTM and NABDY introduce a perspective on quantum dynamics distinctly different from traditional basis set methods. The equations of motion entirely avoids the issue of integration over basis functions. An immediate benefit is that the potential energy surface information is only required at the fluid element positions. Also, the fluid dynamical definition of the velocity couples the velocities of different fluid elements, introducing a quantum mechanical component of the trajectory propagation, in contrast to independent, classical trajectories.

Nevertheless, we still need to evaluate spatial derivatives of the wave function, just as is required for the kinetic energy operator in a typical basis set expansion. Pseudospectral methods offer highly accurate spatial derivatives for the time-dependent Schrödinger equation on time-independent, structured grids optimized based on principles such as Gaussian quadrature.[1]

2.7 Conclusion

Having introduced Ehrenfest trajectories, FSSH, AIMS, and NABDY, we are at a crossroads of seemingly disparate methods for nonadiabatic dynamics. While independent trajectories are a natural predecessor to methods such as AIMS, our interest in describing complicated quantum dynamics demands a more sophisticated method. Both AIMS and NABDY have the attractive feature that the quantum mechanics is only ever (in principle) solved in regions with non-negligible amplitude. AIMS exploits the simplicity of Gaussian trajectories to effi-

ciently run dynamics in an arbitrary number of dimensions. In contrast, NABDY discretizes the wave function, simplifying the equations of motion but imposing a challenging numerical task. In my thesis, we pursue a method that adopts ideas from both Gaussian-based methods and Bohmian mechanics to achieve simple, accurate, and robust dynamics.

We introduce a pseudospectral trajectory-guided Gaussian method. We demonstrate on a series of model potentials that the pseudospectral representation of the unstructured, independently swarm of Gaussian basis functions is capable of achieving quantitative accuracy in describing strong quantum mechanical effects. We employ a matrix equation for the TDSE, similar to AIMS, but avoid the challenges of integration. We adopt a grid representation, but avoid the Bohmian ansatz that leads to numerically unstable equations of motion. An important distinction between Bohmian mechanics and the Gaussian-based methods is that the amplitude has a spatial dependence. In a basis set expansion, the coefficients $c(t)$ do not have a spatial component. This considerably reduces the complexity of the kinetic energy operator and entirely avoids the quantum potential.

2.8 References

[1] D. Tannor, *Introduction to Quantum Mechanics: A Time-dependent Perspective* (University Science Books, 2007), ISBN 9781891389238.

[2] F. F. de Carvalho, M. E. F. Bouduban, B. F. E. Curchod, and I. Tavernelli, Entropy **16**, 62 (2013), ISSN 1099-4300.

[3] M. Born and K. Huang, *Dynamical Theory of Crystal Lattices*, International series of monographs on physics (Clarendon Press, 1998).

[4] J. C. Burant and J. C. Tully, The Journal of Chemical Physics **112**, 6097 (2000).

[5] T. Van Voorhis, T. Kowalczyk, B. Kaduk, L.-P. Wang, C.-L. Cheng, and Q. Wu, Ann. Rev. Phys. Chem. **61**, 149 (2010).

[6] T. Pacher, L. Cederbaum, and H. Köppel, J. Chem. Phys. **89**, 7367 (1988).

[7] T. Pacher, H. Köppel, and L. Cederbaum, J. Chem. Phys. **95**, 6668 (1991).

[8] M. Baer and R. Englman, Mol. Phys. **75**, 293 (1992).

[9] T. Pacher, L. S. Cederbaum, and H. Köppel, Adv. Chem. Phys. **84**, 293 (1993).

[10] K. Ruedenberg and G. Atchity, J. Chem. Phys. **99**, 3799 (1993).

[11] A. Thiel and H. Köppel, J. Chem. Phys. **110**, 9371 (1999).

[12] Y. Kim, J. Corchado, J. Villà, J. Xing, and D. Truhlar, J. Chem. Phys. **112**, 2718 (2000).

[13] H. Köppel, J. Gronki, and S. Mahapatra, J. Chem. Phys. **115**, 2377 (2001).

[14] J. Subotnik, S. Yeganeh, R. Cave, and M. Ratner, J. Chem. Phys. **129**, 244101 (2008).

[15] L. Song and J. Gao, J. Phys. Chem. A **112**, 12925 (2008).

[16] J. C. Tully, Faraday Discuss. **110**, 407 (1998).

[17] J. C. Tully, J. Chem. Phys. **93**, 1061 (1990).

[18] O. V. Prezhdo and P. J. Rossky, J. Chem. Phys. **107**, 825 (1997).

[19] D. M. Kernan, G. Ciccotti, and R. Kapral, J. Chem. Phys. **116**, 2346 (2002).

[20] R. Kapral, Annu. Rev. Phys. Chem. **57**, 129 (2006).

[21] N. Shenvi, J. E. Subotnik, and W. Yang, J. Chem. Phys. **135**, 024101 (2011).

[22] J. E. Subotnik, J. Phys. Chem. A **115**, 12083 (2011).

[23] J. E. Subotnik and N. Shenvi, J. Chem. Phys. **134**, 024105 (2011).

[24] N. Shenvi, J. E. Subotnik, and W. Yang, J. Chem. Phys. **134**, 144102 (2011).

[25] B. R. Landry and J. E. Subotnik, J. Chem. Phys. **137**, 22A513 (2012).

[26] B. F. E. Curchod and I. Tavernelli, The Journal of Chemical Physics **138**, 184112 (pages 18) (2013).

[27] E. R. Bittner and P. J. Rossky, J. Chem. Phys. **103**, 8130 (1995).

[28] G. Granucci, M. Persico, and A. Zoccante, J. Chem. Phys. **133** (2010).

[29] T. J. Martínez, M. Ben-Nun, and R. D. Levine, J. Phys. Chem. **100**, 7884 (1996).

[30] T. J. Martínez, M. Ben-Nun, and G. Ashkenazi, J. Chem. Phys. **104**, 2847 (1996).

[31] T. J. Martínez, M. Ben-Nun, and R. D. Levine, J. Phys. Chem. A **101**, 6389 (1997).

[32] M. Ben-Nun and T. J. Martínez, J. Chem. Phys. **108**, 7244 (1998).

[33] M. Ben-Nun and T. J. Martínez, Chem. Phys. Lett. **298**, 57 (1998).

[34] M. Ben-Nun and T. J. Martínez, J. Chem. Phys. **110**, 4134 (1999).

[35] M. Ben-Nun, J. Quenneville, and T. J. Martínez, J. Phys. Chem. A **104**, 5161 (2000).

[36] M. Ben-Nun and T. J. Martínez, Adv. Chem. Phys. **121**, 439 (2002).

[37] B. G. Levine, J. D. Coe, A. M. Virshup, and T. J. Martínez, Chem. Phys. **347**, 3 (2008).

[38] D. Makhov, K. Saita, T. J. Martínez, and D. Shalashilin, Phys. Chem. Chem. Phys. **17**, 3316 (2014).

[39] D. V. Makhov, W. J. Glover, T. J. Martínez, and D. V. Shalashilin, J. Chem. Phys. **141**, 054110 (2014).

[40] D. Huber and E. J. Heller, J. Chem. Phys. **89**, 4752 (1988).

[41] D. Huber, S. Ling, D. G. Imre, and E. J. Heller, J. Chem. Phys. **90**, 7317 (1989).

[42] D. V. Shalashilin and M. S. Child, J. Chem. Phys. **113**, 10028 (2000).

[43] G. A. Worth and I. Burghardt, Chem. Phys. Lett. **368**, 502 (2003).

[44] Y. Wu and V. S. Batista, J. Chem. Phys. **118**, 6720 (2003).

[45] Y. Wu and V. S. Batista, J. Chem. Phys. **121**, 1676 (2004).

[46] D. V. Shalashilin and M. S. Child, Chem. Phys. **304**, 103 (2004).

[47] B. Hartke, Phys. Chem. Chem. Phys. **8**, 3627 (2006).

[48] S. Habershon, J. Chem. Phys. **136**, (2012).

[49] W. Koch and T. J. Frankcombe, Phys. Rev. Lett. **110**, 263202 (2013).

[50] M. A. C. Saller and S. Habershon, J. Chem. Theory Comput. **11**, 8 (2015).

[51] E. J. Heller, J. Chem. Phys. **62**, 1544 (1975).

[52] B. Lasorne, M. A. Robb, and G. A. Worth, Phys. Chem. Chem. Phys. **9**, 3210 (2007).

[53] B. F. E. Curchod, I. Tavernelli, and U. Rothlisberger, Phys. Chem. Chem. Phys. **13**, 3231 (2011).

[54] C. L. Lopreore and R. E. Wyatt, Phys. Rev. Lett. **82**, 5190 (1999).

[55] R. E. Wyatt, D. J. Kouri, and D. K. Hoffman, J. Chem. Phys. **112**, 10730 (2000).

[56] R. E. Wyatt and E. R. Bittner, J. Chem. Phys. **113**, 8898 (2000).

[57] X.-G. Hu, T.-S. Ho, H. Rabitz, and A. Askar, Phys. Rev. E **61**, 5967 (2000).

[58] X.-G. Hu, T.-S. Ho, H. Rabitz, and A. Askar, Comput. Math. Appl. **43**, 525 (2002).

[59] B. K. Kendrick, J. Chem. Phys. **119**, 5805 (2003).

[60] R. Wyatt and C. Trahan, *Quantum Dynamics with Trajectories: Introduction to Quantum Hydrodynamics*, Interdisciplinary applied mathematics (Springer, 2006).

CHAPTER 3

ASSESSMENT OF DELOCALIZATION ERROR IN PARAMETRIC 2-RDM

3.1 Introduction

In electronic structure theory, methods and models are developed to describe properties of molecules and materials based on an accurate description of electrons. Perhaps the most important properties calculated in electronic structure theory are electronic state energies. We can use energies to answer questions regarding reaction pathways, electronic excitations, conformer analysis and many other issues important to chemists. However, energies are but one component of electronic structure calculations. Ideally, we can use the calculation to determine relative atomic charges, dipole moments and the nature of chemical bonds. Of course, the calculation of the energy and other molecular properties is closely related, but accurate properties do not necessarily follow from accurate energies because of issues such as cancellation of errors. [1] In this chapter, we investigate the quality of the one-electron density calculated from the parametric two-electron reduced-density-matrix (p2-RDM) method. In particular, we explore cases where electron delocalization significantly affects the character of the system, posing difficulties for some electronic structure methods.

A promising alternative to wave function-based and density functional theory (DFT) electronic structure theory methods are based on the direct determination of the two-electron reduced-density-matrix (2-RDM) without knowledge of the many-electron wave function.[2–10] Since electrons interact through at most pairwise interactions, the energy of an N-electron system may be calculated from the 2-RDM without approximation. The 2-RDM grows polynomially with system size, making it a desirable starting point for electronic structure calculations since the N-electron wave function grows exponentially with system size.

The energy for the system may be written as a linear functional of the 2-RDM, allowing a direct variational minimization of the energy with respect to the 2-RDM. If one attempts

to minimize the energy, there are constraints that must be placed on the 2-RDM to ensure it corresponds to a real N-body wave function, including hermiticity and permutational symmetry.[2, 9, 10] However, an attempt to minimize the energy based on the basic constraints of a fermionic system will yield an energy well below the true ground state energy. This is because there are many 2-RDMs that satisfy the constraints but do not reflect the true wave function. The problem of finding a 2-RDM corresponding to a real wave function is known as N-representability. The N-representability conditions required to ensure the 2-RDM is N-representable are nontrivial.

One approach to overcoming the N-representability problem is a hierarchy of conditions known as p-positivity, where p-RDMs are enforced to be positive semidefinite. A subset, known as 2-positivity, is capable of calculating accurate molecular energies. [11–14] However, full implementation of 2-positivity requires the solution of a semidefinite problem, which becomes computationally prohibitive for large systems. The computational cost may be reduced if we parameterize the 2-RDM and relax the 2-positive constraints. The p2-RDM method is based on ideas similar to a configuration interaction singles-doubles (CISD), is capable of calculating accurate energies and nearly N-representable 2-RDMs.[15–18]

While the p2-RDM method has been successfully applied to a variety of molecular systems, we are interested in a particular class of problems prevalent in electronic structure theory, delocalization of electrons. The delocalization of electrons is a hallmark of quantum mechanics and essential in understanding aromaticity and transition metal chemistry. However, the delocalization of electrons presents a significant challenge to both DFT and 2-RDM methods. [19–22]

The literature on delocalization error stems from early discussions on fractional charge in DFT.[23, 24] Perdew et al. proved that the energy of a system with respect to particle number N should be piecewise-linear with derivative discontinuities at integer N. Delocalization (localization) error arises when the energy between integer N is convex (concave) rather than linear. Although we study systems of fixed, integer values of N, the connection between

this work and the discussion of fractional charge is clear if we consider the partitioning of a total system into subsystems. Since the electron density is a continuous function of three-dimensional space, the electrons may be distributed diffusely, appearing as fractionally charged in particular regions of space.

In DFT, the system is described exclusively through the diagonal elements of the 1-RDM (the density). The density is easily enforced to be N-representable. The error arises in the calculation of the energy using only the density. The Hamiltonian formally requires all of the information of the 2-RDM (diagonal and off-diagonal elements) to calculate the energy exactly. Therefore, the error in DFT arises in the approximate energy functionals used to calculate the energy, not from N-representability. In contrast, the energy may be calculated exactly from the 2-RDM, but error arises from incomplete N-representability conditions. In both cases, delocalization of electrons have proven to drive the methods to qualitative failure.

In this work we evaluate the susceptibility of the parametric 2-RDM method to delocalization error by illustrative cases used frequently in the DFT literature. These include diatomic dissociation (BeH^+, HF, Ne_2^+), [10]annulene conformers, chains of hydrogen dimers, and ionization of a 2-D helium lattice. In the diatomic dissociations, parametric 2-RDM successfully predicts the potential energy surface *and* the Mulliken populations on each atom in the dissociated limit. Additionally, parametric 2-RDM has errors comparable to or less than CCSD in the prediction of [10]annulene conformers and the atomization/adhesion energies of hydrogen dimers. Finally, the ionization of the helium lattice visualizes the discrepancies seen in the previous sections by contrasting parametric 2-RDM with Hartree-Fock and DFT. Coupled cluster methods have been used previously as a benchmark because, as wave function methods, have demonstrated proper treatment of delocalized systems. Therefore, the ability of parametric 2-RDM to remain competitive in these particularly challenging systems is promising for its utility in future work.

3.2 Theory

3.2.1 Energy Functional

Since electrons interact through at most pairwise interactions, we may write the energy as a function of a reduced Hamiltonian (${}^2K$) rather than the N-particle Hamiltonian using the following expression

$$E = \sum_{pq} {}^1K^p_q \, {}^1D^p_q + \sum_{pqst} {}^2V^{pq}_{st} \, {}^2D^{pq}_{st} \tag{3.1}$$

$$E = \mathrm{Tr}({}^2K \, {}^2D), \tag{3.2}$$

where ${}^1D^p_q$ and ${}^2D^{pq}_{st}$ are the one and two-electron reduced density matrices which are normalized to N and $N(N-1)$, respectively. The elements of the reduced Hamiltonian matrix (${}^2K$) are defined from the reduced Hamiltonian operator

$${}^2\hat{K} = \frac{1}{N-1}\left(-\frac{1}{2}\nabla^2_1 - \sum_k \frac{Z_k}{r_{1k}}\right) + \frac{1}{2}\frac{1}{r_{12}}. \tag{3.3}$$

In a finite orbital basis, the elements of ${}^2\hat{K}$ are simply the one- and two-electron integrals labeled as ${}^1K^p_q$ and ${}^2V^{pq}_{st}$ in Equation 3.1, respectively. The parametric 2-RDM method calculates ${}^2D$ and consequently the energy directly and without knowledge of the N-particle wave function.

3.2.2 2-RDM Parametrization

The 2-RDM may be expressed as the sum of an anti-symmetric product of the 1-RDM and a cumulant (or connected) part that is not contained in the 1-RDM.

$${}^2D^{pq}_{st} = {}^1D^p_s \, {}^1D^q_t - {}^1D^p_t \, {}^1D^q_s + {}^2\Delta^{pq}_{st}. \tag{3.4}$$

Similarly, the 1-RDM may be partitioned into a diagonal mean-field matrix and a correlated matrix that connects multiple determinants,

$$ {}^1D_q^p = \left({}^1D_o\right)_q^p + {}^1\Delta_q^p. \tag{3.5} $$

The correlated parts of both the 1- and 2-RDMs may be decomposed into two Hermitian matrices,

$$ {}^1\Delta = {}^1T + {}^1R, \tag{3.6} $$

$$ {}^2\Delta = {}^2T + {}^2R, \tag{3.7} $$

where ${}^2T$ represents the first-order part of ${}^2\Delta$, T^1 is the second order part of ${}^1\Delta$ (the first-order part of ${}^1\Delta$ vanishes), and ${}^2R$ and ${}^1R$ contain higher-order corrections within a renormalized perturbation theory. We can then derive part of ${}^2R$ and ${}^1R$ in terms of ${}^2T$ and ${}^1T$. However, this functional is not N-representable.

3.2.3 2-RDM N-Representability

In order to enforce approximate N-representability of the 2-RDM we consider a set of necessary conditions known as two-positivity that enforce the positive semi-definiteness of the two-particle, two-hole, and particle-hole matrices,

$$ {}^2D \succeq 0 \tag{3.8} $$

$$ {}^2Q \succeq 0 \tag{3.9} $$

$$ {}^2G \succeq 0 \tag{3.10} $$

Table 3.1: Values for the topological factor for the following four methods: configuration interaction doubles (CID), coupled electron pair approximation (CEPA), and the 2-RDM methods, K and M.

	Topological factor for case n_o/n_v								
Method	0/0	1/0	2/0	0/1	0/2	1/1	2/1	1/2	2/2
CID	1	1	1	1	1	1	1	1	1
CEPA	0	0	0	0	0	0	0	0	0
K	0	1/2	1	1/2	1	3/4	1	1	1
M	0	0	1	0	1	1	1	1	1

The 2-positivity conditions imply a set of Cauchy-Schwarz inequalities,

$$\left({}^2D^{ij}_{ab}\right)^2 \leq {}^2D^{ij}_{ij}\,{}^2D^{ab}_{ab} \tag{3.11}$$

$$\left({}^2Q^{ij}_{ab}\right)^2 \leq {}^2Q^{ij}_{ij}\,{}^2Q^{ab}_{ab} \tag{3.12}$$

$$\left({}^2G^{ia}_{bj}\right)^2 \leq {}^2G^{ia}_{ia}\,{}^2G^{bj}_{bj} \tag{3.13}$$

where the last inequality represents one of four distinct inequalities for the ${}^2G$ matrix.

Substituting the definitions of the 2-RDM elements into these inequalities and equating the connected parts give 2-RDM elements that satisfy two-positivity. Taking different averages of the six size extensive equations yields the topological factors introduced by Kollmar and Mazziotti. The general expression for the connected elements is

$${}^2\Delta^{ab}_{ij} = {}^2T^{ab}_{ij}\sqrt{1 - \frac{1}{4}\sum_{cdkl} f^{ijkl}_{abcd} \mid {}^2T^{cd}_{kl} \mid^2}. \tag{3.14}$$

where f^{ijkl}_{abcd} is known as the topological factor and adopts different values for different parameterizations. Since f only depends on the number of indices shared between ${}^2T^{ab}_{ij}$ and ${}^2T^{cd}_{kl}$ its values may be divide into nine classes, labeled by n_o/n_v where n_o is the number of occupied orbitals shared by $\{ij\}$ and $\{kl\}$ and n_v is the number of virtual orbitals $\{ab\}$ and $\{cd\}$. Table 3.1 defines the topological factor for CID, coupled electron pair approximation

(CEPA), the parameterization derived by Kollmar (K) [15], and Mazziotti (M) [17]. The work presented here exclusively uses the M functional when referring to parametric 2-RDM calculations.

3.2.4 Delocalization Error

Delocalization error is a manifestation of the fact that an electronic structure method does not linearly interpolate the electronic energy between integer numbers of electrons. Perdew *et al.* proved in 1982 that the energy should be a linear piecewise function between electrons, with a derivative discontinuity at integer electron number.[24] Consider a system of $N = M + \omega$ electrons where M is an integer and $0 \leq \omega \leq 1$. The energy may be minimized over a statistical mixture of densities corresponding to Ψ_M and Ψ_{M+1}, states of M and $M+1$ electrons, respectively. The probabilities will now be $1-\omega$ and ω, where $(1-\omega)M + \omega(M+1) = M + \omega$. The Energy may be written as a statistical mixture

$$E = (1-\omega)E_M + \omega E_{M+1}. \tag{3.15}$$

Clearly, the energy of a fractionally charged system should vary linearly between electron number because any partially occupied state may be written as a linear combination of the M and $M+1$-electron states.

In practice, however, this is not observed. The vast majority of DFT functionals produce a convex function from M to $M+1$. As a result, a system with a fractional number of electrons maybe lower than either E_M or E_{M+1}. The origin of the error in DFT arises from a non-zero interaction term between an electron and itself, known as self-interaction error.[23, 25] Formally, the exact functional would be self-interaction free, but DFT functionals are, in general, not free of self-interaction error. Although one rarely calculates the energy of a non-integer electron system, the manifestation of self-interaction error is readily observed in molecular systems. If the molecular structure may accommodate electron delocalization, the

extent of delocalization will be exaggerated in the density distribution and the energy will be lowered by the spatially diffuse electron density.. [19, 20, 24, 26]

In 2-RDM methods, there is not self-interaction error because the energy of an N-electron system is calculated without approximation. However, it has been reported that the variational 2-RDM method exhibits energy convexity similar to DFT. [21, 27–29] Evidence and experience suggests that a violation in N-representability is responsible for the lower energy. The problem has been corrected in small systems using a density partition scheme to enforce integer electron number.[28, 29] However, it is not clear how to partition complicated molecules and the errors suggest an underlying violation of N-representability that is unaccounted for.

We are interested in the extent of delocalization error in the p2-RDM. Although beginning from a Hartree-Fock reference, the p2-RDM is capable of describing unexpectedly strong correlation from a mean field guess. Systems particularly susceptible to delocalization error are investigated and we evaluate a) if p2-RDM is capable of describing the energy and b) if the calculated density properly reflects the underlying chemistry.

3.2.5 Delocalization Metrics

All one-electron properties were calculated from the orthogonalized atomic orbital (AO) 1-RDM, ${}^1D$. The molecular orbital (MO) 1-RDM arises from the contraction of the 2-RDM

$$ {}^1D^i_k = \frac{1}{N-1} \sum_j {}^2D^{ij}_{kj} \tag{3.16} $$

The transformation from the MO to AO density matrix is accomplished through the transformation

$$ {}^1\mathrm{D}^{\mathrm{AO}} = \mathrm{C}\,{}^1\mathrm{D}^{\mathrm{MO}}\mathrm{C}^{\mathrm{T}} \tag{3.17} $$

where C is the matrix of expansion coefficients of the MOs (ϕ_P) expanded in AOs (χ_μ)

$$\phi_P = \sum_\mu C_{\mu P} \chi_\mu. \tag{3.18}$$

Greek letters indicate atomic orbitals. However, equation (3.17) does not produce an orthogonal AO density matrix. Recalling the orthonormality condition for the AOs,

$$\mathrm{C^T S C = I} \tag{3.19}$$

where S is the overlap matrix, we may write

$$^1\mathrm{D^{AO}\ S = C\,{}^1D^{MO}C^{-1}} \tag{3.20}$$

which constitutes a similarity transformation. [30] Consequently, the quantity $^1\mathrm{D^{AO}}$ S satisfies the trace and idempotency conditions of the MO density-matrix and will be used in our analyses; hereafter referred to as ^{1}D.

Mulliken population analyses (MPA) are calculated by summing the diagonal elements of ^{1}D corresponding to basis functions centered on atom i,

$$n_i = \sum_\mu {}^1\mathrm{D}^{\mu,i}_{\mu,i}. \tag{3.21}$$

Although MPAs have been shown to have a significant basis set dependence and inconsistencies in molecules, our emphasis on dissociated geometries avoids these problems because of minimal overlap between atomic basis functions.[20]

3.2.6 Computational Details

All parametric 2-RDM calculations were run using an in-house implementation of the methodology in Ref. [17] The GAMESS electronic structure package was used for all DFT and full

configuration interaction (FCI) calculations. [31, 32] CCSD and CCSD(T) calculations were run using either the Psi4 program [33, 34] or GAMESS[35–37], depending on the application. The aug-cc-pVDZ was used in diatomic dissociations and hydrogen chains, though in the latter case the most diffuse S orbital was removed to avoid possible linear dependence in the basis set, as mentioned in Ref. [38, 39] The cc-pVDZ basis set was used in the [10]annulene study and the 6-31G basis for the helium lattice. [39, 40]

3.3 Applications

Results are presented from three separate studies that probe delocalization error. First, the diatomic dissociation of BeH^+, Ne_2^+ and HF are investigated by Mulliken population analyses and potential energy curves. Second, the relative errors of atomization and adhesion energies of linear chains of hydrogen dimers are presented. Third, parametric 2-RDM data is presented on the long-standing discussion of relative annulene conformers. Finally, electron density difference plots of ionized helium lattices are compared as a measure of electron delocalization.

3.3.1 Diatomic Dissociation

The effects of delocalization error may be observed in diatomic dissociation through potential energy surfaces and atomic population analyses. Given a neutral diatomic molecule XY, the dissociated species should be X^0 and Y^0 if the ionization energy of X is greater than the electron affinity of Y. Since the largest electron affinity on the periodic table [A(Cl)=3.62 eV] is smaller than the smallest ionization energy [I(Cs)=389 eV], any neutral diatomic species will dissociate to neutral products. However, DFT and variational 2-RDM do not reproduce this fundamental behavior and consequently we are interested to see whether parametric 2-RDM will successfully describe dissociation. In these other cases, the dissociated species are X^{+a} and Y^{-a} where $0 < a < 1$. Diatomic dissociations test the ability of parametric

2-RDM to properly describe an ensemble of non-interacting subsystems.

Dissociation of HF

The dissociation of fluoride species has been studied extensively as a metric for DFA performance. Here we extend the study to parametric 2-RDM in order to compare the delocalization error to DFAs. The Mulliken charges on F from R(H-F)= 0.5 Å to 20 Å are presented in Figure 3.1. While there is reasonable agreement for R $<$ 5 Å , only parametric 2-RDM successfully predicts the dissociation to neutral species. At 20 Å parametric 2-RDM predicts $F^{.0162}$ while B3LYP and M06-2X are significantly affected by spurious fractional charge, predicting $F^{-.2240}$ and $F^{-.2608}$, respectively.

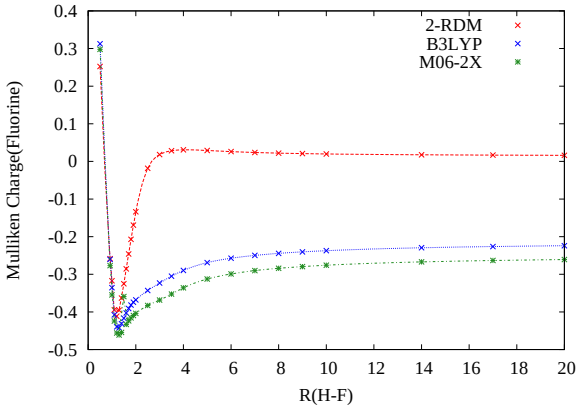

Figure 3.1: Mulliken charge on fluorine in HF as a function of internuclear distance. Parametric2-RDM properly predicts zero charge on fluorine at large R. Additionally, the sharp change in the Mulliken charge at $\approx$ 3 Å is the proper description of charge transfer in the dissociation of a covalent species.

Parametric 2-RDM and CCSD are in agreement across the entire potential energy surface. It is interesting to note that the M06-2X energy approaches that of Parametric 2-RDM despite the persistence of fractional charge in the dissociation limit.

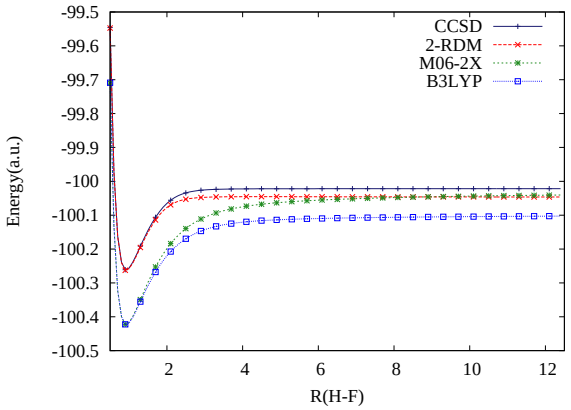

Figure 3.2: Potential energy curve for the dissociation of HF. In addition to properly predicting the charge of the species, parametric 2-RDM accurately predicts the potential energy surface of HF

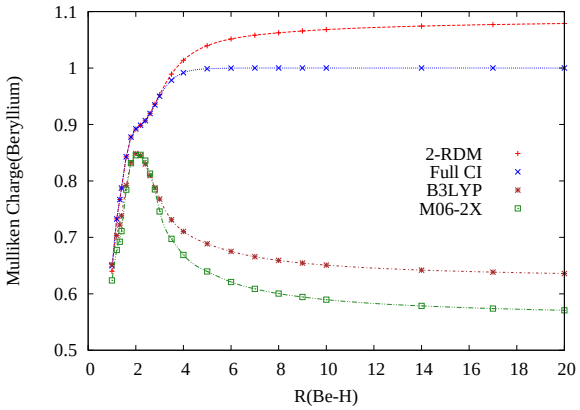

Figure 3.3: Mulliken charge on Beryllium in BeH^+ as a function of internuclear distance.

Dissociation of BeH^+

BeH^+ is a second heteronuclear diatomic that can demonstrate delocalization error in dissociation. The dissociated products should be Be^+ and H because the electron affinity of Be^+ (-9.3227 eV) is less than the ionization energy of H (13.598 eV). The Mulliken charge of Be is presented in Figure 3.3 All methods predict a strongly covalent bond near equilibrium, but only parametric 2-RDM and Full CI predict the increasingly positive charge in the dissociation limit. In the DFT example, the charge transfer to hydrogen reaches a critical point near 2 Å after which the Be regains a substantial negative charge. At 20 Å parametric 2-RDM predicts $Be^{1.080+}$, B3LYP predicts $Be^{.364+}$, M06-2X predicts $Be^{.429+}$, and full CI

Table 3.2: The energies of dissociated (20 Å) and isolated species. The difference in DFT is attributed to the improper treatment of the effective 1/2 charge on Ne in the dissociated limit. Parametric 2-RDM and CCSD correctly predict the energy of the dissociated species as the sum of the two isolated species.

Size Consistency in Ne_2^+ Dissociation			
Method	$E(Ne^+)+E(Ne)$ (a.u.)	$E(Ne–Ne^+)$ (a.u)	Difference (mH)
2-RDM	-256.63243	-256.63134	-1.09561
CCSD	-256.62688	-256.62659	-0.29417
B3LYP	-256.98027	-257.08979	109.51806

predicts Be^+ exactly. Similar to HF, parametric 2-RDM produces a dissociated species with nearly the correct charge. Additionally, the small error is opposite in sign to the spurious fractional charge in DFT.

3.3.2 Dissociation of Ne_2^+

The dissociation of symmetric radical cations have also been studied frequently in DFT and offer a unique perspective because of the degeneracy in the dissociation limit. The dissociation of Ne_2^+ will produce a linear combination of states, $Ne_2^+ \rightarrow \left(Ne_a{}^+ + Ne_b \leftrightarrow Ne_a + Ne_b{}^+\right)$ where a and b denote permutations of the nuclei. The density matrix captures this as the effective linear combination $Ne_2^+ \rightarrow Ne^{+1/2} + Ne^{+1/2}$. While all methods correctly predict the $+1/2$ charge on each neon, the relative energies differ considerably. Given that the function of E vs. N should be piecewise linear, $E(2\,Ne^{+1/2})$ should equal $E(Ne + Ne^+)$. Consequently, the dissociated species may be viewed as a test of the parametric 2-RDM method at fractional values of N. Table 3.2 Clearly shows that the parametric 2-RDM is able to accurately calculate the energy for fractionally charged neon atoms. The ability to capture the linear interpolation between integer values of N may also be viewed as a test of size consistency. Table 3.2 presents data for the isolated species and the molecule at R = 20 Å. Both parametric 2-RDM and CCSD nearly recover the isolated energies in the dissociation limit while there is considerable error in DFT. Additionally, Figure 3.5 uses the dissociated

species as a means of calculating an effective atomic energy for $Ne^{-1/2}$ and $Ne^{+1/2}$. The plot offers a visualization of 2-RDM(M)'s approximate linearity indicated by Table 3.2.

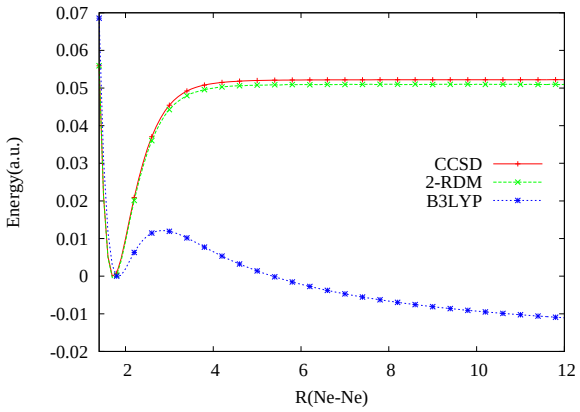

Figure 3.4: The dissociation curve for Ne_2^+. All energies are plotted relative to the equilibrium geometry energy. Parametric 2-RDM correctly describes the dissociation. B3LYP predicts a spurious global minimum at large R caused by the delocalization error.

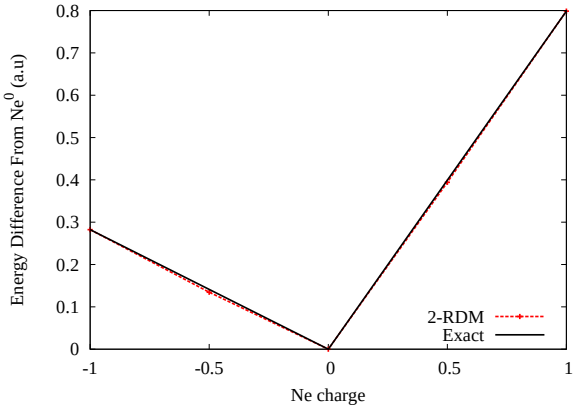

Figure 3.5: The energy of a neon atom as a function of charge. The value for $Ne^{+1/2}$ and $Ne^{-1/2}$ is found by taking 1/2 the total energy of the dissociated products of Ne_2^+ and Ne_2^-, respectively. The integer values of charge were taken from the dissociated species of Ne_2^{2+}, Ne_2 and Ne_2^{2-}. The "Exact" curve is a linear interpolation of the energy at integer charges.

3.3.3 Molecular Hydrogen Chains $(H_2)_n$

We also studied a linear chain of molecular hydrogen molecules as presented in Reference [38]. We report adhesion and atomization data for chains up to $n = 8$ at an intermolecular distance

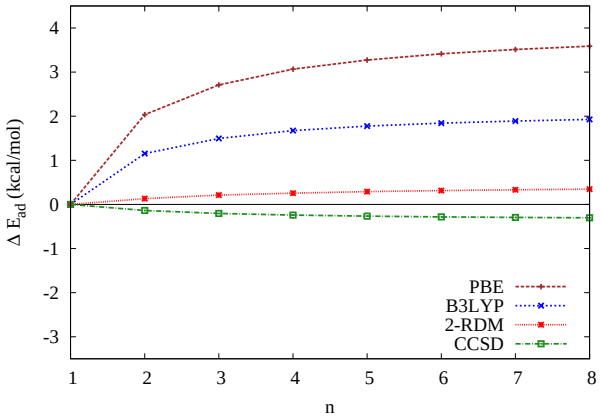

(a) The relative error in adhesion energy with respect to CCSD(T) as a function of chain length n.

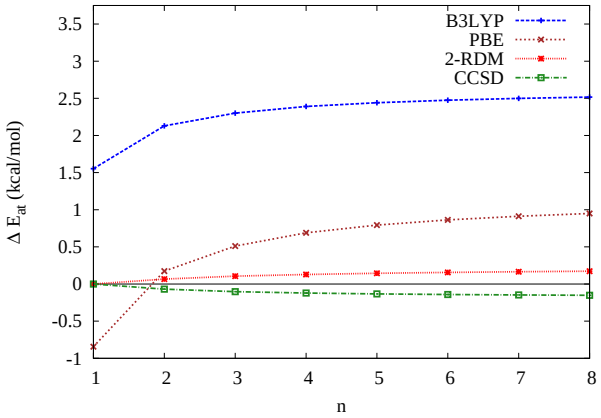

(b) The relative error in atomization energy with respect to CCSD(T) as a function of chain length n.

Figure 3.6: Adhesion and atomization energy errors for linear chains of molecular hydrogen. Deviation above (below) 0 indicates an overestimation (underestimation) of the energy with respect to CCSD(T). In both cases the overestimation of the energies by parametric 2-RDM is on the order of the underestimation by CCSD.

$d = 2.25$ Bohr. The atomization energy is defined as $E_{\text{at}} = 2nE(\text{H}) - E(\text{H}_{2n})$ and adhesion energy $E_{\text{ad}} = nE(\text{H}_2) - E(\text{H}_{2n})$. All data is presented as relative error per H_2 unit from the CCSD(T) reference ($\Delta E^{\text{P2RDM}} = [E^{\text{P2RDM}} - E^{\text{CCSD(T)}}]/2n$).

In Figures 3.6a and 3.6b values greater than (less than) 0 correspond to an overestimation (underestimation)of atomization and adhesion energies relative to CCSD(T) and consequently a measure of delocalization (localization) error. Note that the atomization energy includes the breaking of the H_2 covalent bond and therefore unique from the adhesion

energies. The largest errors for parametric 2-RDM and CCSD atomization energies are 0.172 and -0.151 kcal/mol, respectively, indicating superior performance to standard DFAs where the errors are on the order of 2-10 kcal/mol. Similarly, the largest errors in adhesion energies for parametric 2-RDM and CCSD are 0.345 and -0.3032 kcal/mol, respectively.

3.3.4 [10]Annulene Conformers

The relative energies of [10]annulene($C_{10}H_{10}$) conformers have frequently been used to assess delocalization error in DFAs. We investigate the relative energies of the heart, twist, and naphthalene-like structures. The energetics are difficult because of the balance of aromatic stabilization and steric hinderance. [10]annulene is able to form a (nearly) planar aromatic structure that follows Hückel's 4n+2 rule (the heart geometry). However, the steric hinderance of ten consecutive *cis* carbon-carbon bonds creates a significant penalty to aromatization. Delocalization error produces an unrealistic stabilization from delocalizing electrons across the pi system, effectively negating the steric hinderance and predicting a lower energy for the heart structure.

In order to compare the relative energies, we used fixed geometry structures optimized at the CCSD(T)/6-31G level of theory. Once again, the parametric 2-RDM performs comparably to CCSD and, more importantly, predicts the proper relative energies of the structures. Based on experimental evidence and CCSD(T), the structures from most to least stable are twist, naphthalene-like, and heart. Consistent with the literature, B3LYP predicts the heart structure to be lowest in disagreement with CCSD(T) and experiment. While other functionals improve upon B3LYP, we wish to emphasize the consistency of Parametric 2RDM with coupled cluster methods rather than the failure of a particular DFA.

3.3.5 2-Dimensional Helium Lattice

We use electron density difference plots to investigate the ionization of an 8×8 helium lattice, $He_{64} \rightarrow He_{64}^{+}$. The He atoms are at a fixed nearest neighbor distance of 2 Å. The

Table 3.3: The relative energies of different [10]annulene conformers. All energies are relative to the twist energy for a given method. p2-RDM predicts the correct relative energies performs competitively with CCSD. B3LYP is reported as an example delocalization error.

Relative Energies (kcal/mol)			
Method	Conformer		
	Twist	Naphthalene-like	Heart
B3LYP	0.00	0.38707	-8.80811
CCSD	0.00	2.05042	8.63694
p2-RDM	0.00	1.94612	7.96167
CCSD(T)	0.00	1.39416	3.33650

ionization of the lattice creates an electron hole that is distributed across the lattice. The extent of delocalization may be measured qualitatively by the relative density across the lattice. In the case of DFT the hole is nearly uniformly distributed across the lattice while HF over-localizes the hole in the center. Our work is restricted to ROHF symmetry and consequently our plots have a nodal plane not present in the unrestricted work of Cohen et al. in Ref. [19] where the same process is studied. Similar to the unrestricted CCSD data in previous work, the parametric 2-RDM finds the proper balance between the two extremes of HF and DFT. Additionally, delocalization error is observed through an underestimation of the ionization energy. PBE and M06-2X predict ionization energies of 345 and 441 kcal/mol, respectively, while CCSD and parametric 2-RDM predict 498 and 500 kcal/mol, respectively. The

3.4 Discussion and Conclusions

The parametric 2-RDM method has demonstrated resilience in preventing delocalization error. We have presented data on four unique systems susceptible to delocalization error and in all cases remained competitive or exceeded the performance of CCSD. Given that these systems have been selected because of the systemic errors observed in other density based methods, it is considered a success for parametric 2-RDM to not suffer from the same

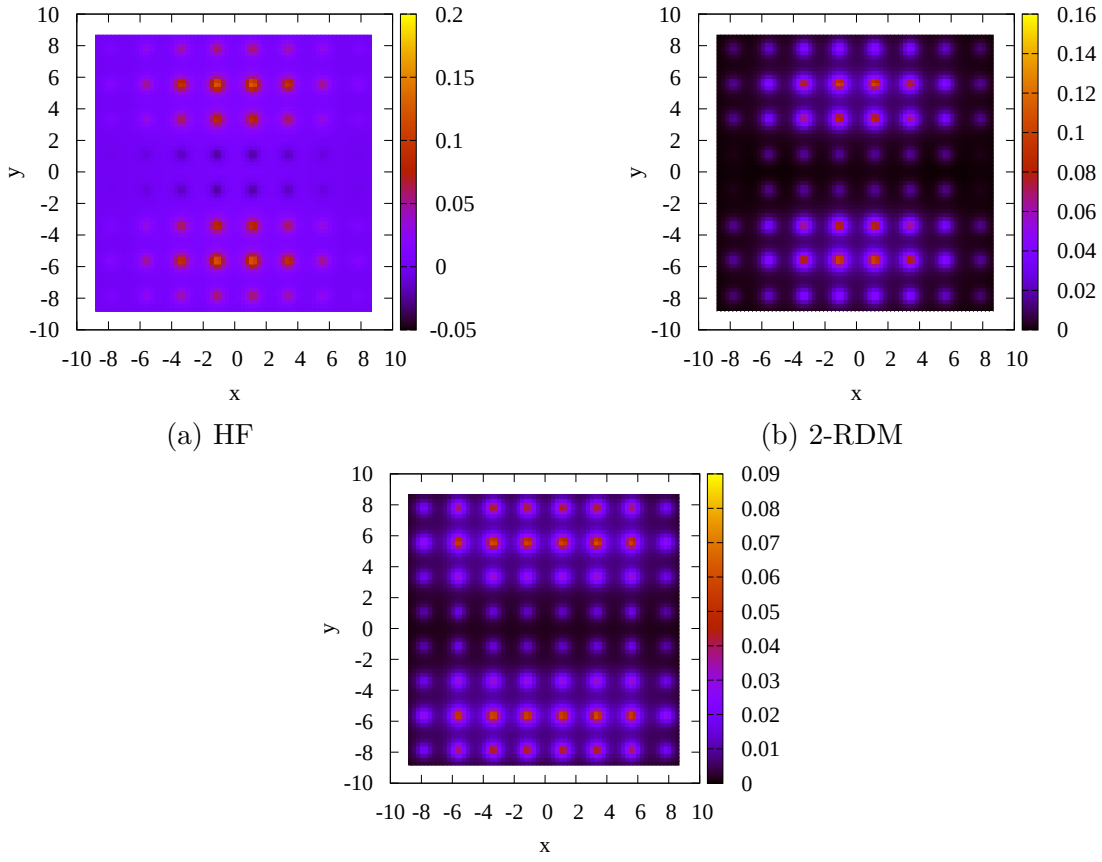

(a) HF

(b) 2-RDM

(c) M06-2X

Figure 3.7: ρ_{hole} as calculated by our code. The distribution of the hole is consistent with Cohen et al. and suggests proper treatment by PRDM. HF localizes the electron density so significantly that a negative region appears in the middle, indicating that the hole localizes so severely that the ionized species actually has a region of higher electron density than the neutral lattice. In contrast, M06-2X has a maximum peak height about 1/2 that of 2-RDM and a near uniform distribution of density along the x-axis.

errors.

The diatomic dissociations indicate that parametric 2-RDM can predict the proper charges on dissociated species and that the method is empirically size-consistent. In both BeH^+ and HF the open shell dissociated products are correctly described by parametric 2-RDM even when starting from an RHF reference. The dissociation of Ne_2^+ highlights the underlying cause of the error in heteronuclear diatomics for DFT. However, the energy of $Ne^{0.5}$ from parametric 2-RDM does not deviate significantly from the linear interpolation. This somewhat contrived example offers validation of parametric 2-RDM's performance in

more chemically relevant applications such as the [10]annulene conformers.

The results of this chapter are also consistent with previous tests of the parametric 2-RDM. Here we have focused exclusively on delocalization error, particularly by studying charge distributions, but the phenomena has been studied implicitly in previous work. In particular, parametric 2-RDM has demonstrated the ability to accurately predict transition state energies and the energies of polyacetylene chains, two examples used in the literature to demonstrate delocalization error. [18, 41–45] The work here offers a general explanation of the success of parametric 2-RDM's well as affirms the prospect of parametric 2-RDM's broad applicability in chemistry.

We have empirically verified that parametric 2-RDM does not suffer from delocalization error. These results are promising for current and future use of the parametric 2-RDM method. While previous work demonstrated that parametric 2-RDM exceeds the accuracy of CCSD in some cases, we have shown parametric 2-RDM does not fail where other density and density-matrix based methods have.

3.5 References

[1] F. Jensen, *Introduction to Computational Chemistry* (John Wiley & Sons, 2006).

[2] A. Coleman, Rev. Mod. Phys. **35**, 668 (1963).

[3] F. Colmenero, C. Perez, and C. Valdemoro, Phys. Rev. A **47**, 971 (1993).

[4] H. Nakatsuji and K. Yasuda, Phys. Rev. Lett. **76**, 1039 (1996).

[5] D. Mazziotti, Int. J. Quantum Chem. **70**, 557 (1998).

[6] D. A. Mazziotti, Phys. Rev. A **65**, 1 (2002).

[7] D. A. Mazziotti, Phys. Rev. A **66**, 1 (2002).

[8] D. A. Mazziotti, Phys. Rev. Lett. **97**, 143002 (2006).

[9] D. Mazziotti, *Advances in Chemical Physics, Reduced-Density-Matrix Mechanics: With Application to Many-Electron Atoms and Molecules*, Advances in Chemical Physics (Wiley, 2007).

[10] A. Coleman and Y. V.I., *Reduced Density Matrices: Coulson's Challenge* (Springer Verlag, 2000).

[11] M. Nakata, H. Nakatsuji, M. Ehara, M. Fukuda, K. Nakata, and K. Fujisawa, J. Chem. Phys. **114**, 8282 (2001).

[12] D. A. Mazziotti, Phys. Rev. Lett. **93**, 19 (2004).

[13] D. A. Mazziotti, Acc. Chem. Res. **39**, 207 (2006).

[14] G. Gidofalvi and D. A. Mazziotti, J. Chem. Phys. **129**, 134108 (2008).

[15] C. Kollmar, J. Chem. Phys. **125**, 084108 (pages 12) (2006).

[16] D. A. Mazziotti, Phys. Rev. Lett. **101**, 253002 (2008).

[17] D. A. Mazziotti, Phys. Rev. A **81**, 062515 (2010).

[18] C. A. Schwerdtfeger, A. E. DePrince, III, and D. A. Mazziotti, J. Chem. Phys. **134**, 174102 (2011).

[19] A. J. Cohen, P. Mori-Sánchez, and W. Yang, Chem. Rev. **112**, 289 (2012).

[20] A. Ruzsinszky, J. P. Perdew, G. I. Csonka, O. A. Vydrov, and G. E. Scuseria, J. Chem. Phys. **125**, 194112 (pages 8) (2006).

[21] H. Van Aggelen, P. Bultinck, B. Verstichel, D. Van Neck, and P. W. Ayers, Phys. Chem. Chem. Phys. **11**, 5558 (2009).

[22] J. M. Matxain, M. Piris, F. Ruiperez, X. Lopez, and J. M. Ugalde, Phys. Chem. Chem. Phys. **13**, 20129 (2011).

[23] J. P. Perdew and A. Zunger, Phys. Rev. B **23**, 5048 (1981).

[24] J. P. Perdew, R. G. Parr, M. Levy, and J. L. Balduz, Phys. Rev. Lett. **49**, 1691 (1982).

[25] J. P. Perdew, Int. J. Quantum Chem. **28**, 497 (1985).

[26] O. A. Vydrov, G. E. Scuseria, and J. P. Perdew, J. Chem. Phys. **126**, 154109 (pages 9) (2007).

[27] W. Yang, Y. Zhang, and P. W. Ayers, Phys. Rev. Lett. **84**, 5172 (2000).

[28] H. van Aggelen, B. Verstichel, P. Bultinck, D. V. Neck, P. W. Ayers, and D. L. Cooper, J. Chem. Phys. **132**, 114112 (pages 10) (2010).

[29] B. Verstichel, H. van Aggelen, D. V. Neck, P. W. Ayers, and P. Bultinck, J. Chem. Phys. **132**, 114113 (pages 6) (2010).

[30] T. Helgaker, P. Jørgensen, and J. Olsen, *Molecular Electronic-Structure Theory* (Wiley, 2000).

[31] M. W. Schmidt, K. K. Baldridge, J. A. Boatz, S. T. Elbert, M. S. Gordon, J. H. Jensen, S. Koseki, N. Matsunaga, K. A. Nguyen, and al. Et, J. Comput. Chem. **14**, 1347 (1993).

[32] M. S. Gordon and M. W. Schmidt, in *Theory and Applications of Computational Chemistry*, edited by C. E. Dykstra, G. Frenking, K. S. Kim, and G. E. Scuseria (Elsevier, Amsterdam, 2005), pp. 1167 – 1189.

[33] J. M. Turney, A. C. Simmonett, R. M. Parrish, E. G. Hohenstein, F. A. Evangelista, J. T. Fermann, B. J. Mintz, L. A. Burns, J. J. Wilke, M. L. Abrams, et al., Wiley Interdisciplinary Reviews: Computational Molecular Science **2**, 556 (2012).

[34] K. B. Lipkowitz, D. B. Boyd, T. D. Crawford, and H. F. S. III, *An Introduction to Coupled Cluster Theory for Computational Chemists* (John Wiley & Sons, Inc., 2007), vol. 14, pp. 33–136.

[35] P. Piecuch, S. A. Kucharski, K. Kowalski, and M. MusiaÅ, Computer Physics Communications **149**, 71 (2002).

[36] K. Kowalski and P. Piecuch, J. Chem. Phys. **120**, 1715 (2004).

[37] M. Włoch, J. R. Gour, K. Kowalski, and P. Piecuch, J. Chem. Phys. **122**, 214107 (pages 15) (2005).

[38] X. Zheng, M. Liu, E. R. Johnson, J. Contreras-García, and W. Yang, J. Chem. Phys. **137**, 214106 (pages 7) (2012).

[39] J. Thom H. Dunning, J. Chem. Phys. **90**, 1007 (1989).

[40] W. J. Hehre, R. Ditchfield, and J. A. Pople, J. Chem. Phys. **56**, 2257 (1972).

[41] A. E. DePrince and I. D. A. Mazziotti, J. Chem. Phys. **133**, 034112 (pages 9) (2010).

[42] A. E. DePrince and I. D. A. Mazziotti, J. Chem. Phys. **132**, 034110 (pages 9) (2010).

[43] A. M. Sand, C. a. Schwerdtfeger, and D. A. Mazziotti, J. Chem. Phys. **136**, 034112 (2012).

[44] E. P. Hoy, C. A. Schwerdtfeger, and D. A. Mazziotti, Molecular Physics **110**, 765 (2012).

[45] T. Korzdorfer, R. M. Parrish, J. S. Sears, C. D. Sherrill, and J.-L. Bredas, J. Chem. Phys. **137**, 124305 (pages 8) (2012).

CHAPTER 4

ADIABATIC PSEUDOSPECTRAL GAUSSIAN DYNAMICS: EFFICIENT SAMPLING OF POTENTIAL ENERGY SURFACES

This chapter contains parts of a paper that, at the time of printing, has been submitted to The Journal of Chemical Physics for publication.

4.1 Introduction

Beginning with the pioneering work of Heller and co-workers, Gaussian wave packets play a central role in many of the most successful methods for high-dimensional quantum molecular dynamics.[1–15] Gaussians are particularly attractive as a basis set because they are localized, analytically integrable for polynomial and exponential potentials and readily propagated using classical equations of motion. Collectively, these features make Gaussian basis sets ideal for "on-the-fly" or direct dynamics, in which the potential energy is determined during the propagation using electronic structure calculations.[16–26] Electronic structure calculations, however, can be computationally expensive in floating-point operations and memory-storage requirements, especially at non-equilibrium geometries and excited states where strong electron correlation can be significant.[27–31] While improvements in electronic structure methods continue to improve the speed and accuracy of quantum molecular dynamics calculations, it is important that molecular dynamics methods be designed to generate accurate time-dependent solutions with minimal sampling of the molecular potential energy surface.

A key ingredient in Gaussian-based quantum molecular dynamics methods (QMD) is the evaluation of matrix elements. In order to evaluate matrix elements a test function needs to be selected. The test function defines the space onto which the approximate solution will be projected. In Gaussian based methods, the wave function is typically tested using the

complex conjugate of the basis functions. Choosing the basis function as the test function, known as the Galerkin method, leads to a Hermitian Hamiltonian and the familiar Rayleigh-Ritz variational principle.[4–6, 8, 12–15, 32–37] Unfortunately, the potential energy integrals, $\int \phi_j^*(x)V(x)\phi_i(x)dx$, are only analytically solvable for particular model surfaces. When dynamics are performed "on-the-fly", where the potential energy is obtained at discrete points through electronic structure calculations, the integrals need to be approximated.

In this work, we test the time-dependent Schrödinger equation (TDSE) not with the Gaussian basis functions but rather with Dirac delta functions that are located at the centers of the Gaussian basis functions.[38–50] Selection of the Dirac delta functions rather than the Gaussian basis functions as the test functions has the significant advantage that the potential only needs to be evaluated at the grid points associated with the Dirac delta functions. Because the number N of test functions equals the number N of basis functions, the sampling of the potential is $\mathcal{O}(N)$. Since the Dirac delta function test function is characteristic of pseudospectral methods, we refer to the new method throughout as the pseudospectral Gaussian method.[38, 51–57]

The time dependence of the basis functions in this chapter is governed by classical mechanics.[2, 5, 6, 8, 58] We wish to emphasize that the arguments regarding test functions and expression of the Hamiltonian are independent of the trajectory choice. More quantum-mechanical equations of motion, such as those the Gaussian-multi-configurational time-dependent Hartree (G-MCTDH) method may further improve results.[11, 12]

An alternative trajectory-based formulation of quantum mechanics is the quantum trajectory method based on the Bohmian wave function ansatz.[59–61] Although we adopt a matrix formulation of the time-dependent Schrödinger equation similar to other Gaussian-based methods, the motivation to discretize the basis arises from Bohmian trajectory methods. Other recent work has also focused on the development of methods that adopt ideas from both Bohmian mechanics and basis set solutions to the time-dependent Schrödinger equation.[24, 62, 63]

There are two principal objectives to this work. First, we demonstrate that testing a time-dependent basis of Gaussians with Dirac delta functions produces an accurate and efficient quantum molecular dynamics method. Given the lack of published literature and the well-known numerical complications of Gaussian basis sets, the positive results in this chapter are promising as an alternative to more traditional Gaussian-based methods. Second, we demonstrate the pseudospectral Gaussian method offers accuracy comparable to variational calculations where the integrals are evaluated analytically. While Yang and Peet originally reported comparable accuracy between collocation and Galerkin Gaussian methods, we believe the implications regarding potential energy sampling have been under appreciated, especially in the context of dynamics.[41–45, 64–66] Recovering the accuracy of analytical integration from only $\mathcal{O}(N)$ potential energy sampling offers significant advantages, particularly for more complicated dynamics. Additionally, we implement the bra-ket averaged Taylor expansion (BAT), a potential energy approximation that requires the same potential energy information as the pseudospectral Gaussian method.[25, 67, 68] While the BAT is sufficient for some classes of dynamics, we find the approximation struggles for more quantum-mechanical processes including barrier reflection.

Before the pseudospectral Gaussian method is applied to time-dependent problems, it is applied to the time-independent problem of computing the vibrational states of a diatomic molecule. Results from the pseudospectral Gaussian method are compared with those from a Gaussian-based Galerkin method. The computed vibrational energies show that the pseudospectral Gaussian method, using Dirac delta functions at equally spaced points, exceeds the accuracy of the Gaussian tests functions with approximate integration by orders of magnitude while achieving comparable accuracy to the variational Gaussian method. Time-dependent applications include molecular oscillations within a one-dimensional Morse potential and a generalized version of the Henon-Heiles potential in two, four, and six dimensions. The resulting time-dependent simulations demonstrate that the pseudospectral Gaussian molecular dynamics yields quantitatively accurate density populations and coher-

ences in cases that are difficult to treat without an accurate representation of the quantum mechanics.

4.2 Theory

The pseudospectral Gaussian method is introduced with a discussion of the test and basis functions in Section 4.2.1, the matrix equations and their solution inSection 4.2.2 and the equations of motion in Section 4.2.3.

4.2.1 Test and Basis Functions

Testing the time-dependent Schrödinger equation with the N_f test functions χ_i yields

$$\left\langle \chi_i(t) \left| i\frac{d}{dt} - \hat{H} \right| \psi(t) \right\rangle = 0. \tag{4.1}$$

The wave function can be expanded in terms of N_f basis functions ϕ_i,

$$|\psi(\mathbf{x},t)\rangle = \sum_{i}^{N_f} c_i(t)\phi_i(\mathbf{x},t). \tag{4.2}$$

If both the basis and test functions are chosen to be Gaussian functions, then the evaluation of the potential requires numerical integration which, without approximation, scales as $\mathcal{O}(N_f^2)$. However, if we choose the test functions to be Dirac delta functions, located at the centers of the Gaussian basis functions, then the evaluation of the potential scales as $\mathcal{O}(N_f)$. The Gaussian functions are chosen to be time-dependent, moving according to Hamilton's equations of motion.

Each basis function, for a problem in N_d-dimensions, is given as a product of one-

dimensional functions

$$\phi_i(\mathbf{x},,t;\alpha_i,\mathbf{x}_i(t),\mathbf{p}_i(t),\gamma_i(t)) = \\ \exp(\gamma_i)\prod_{k=1}^{N_d}\exp(-\alpha_{i_k}(\Delta x_{i_k})^2 + ip_{i_k}(\Delta x_{i_k})), \tag{4.3}$$

where the width $\Delta x_{i_k} = (x_k - x_{i_k})$ is time-independent (frozen Gaussians) and γ_i is complex, accounting for phase and normalization. N_f is the basis set size while N_d is the number of degrees of freedom in the system. Therefore, $\mathbf{x}_i$ and $\mathbf{p}_i$ represent the N_d-dimensional vectors corresponding to the time-dependent basis function position and momentum centers for the ith basis function.

4.2.2 Matrix Equations and their Solution

Assigning the N_d-dimensional Dirac delta function to the test function

$$|\chi_i\rangle = \delta(\mathbf{x} - \mathbf{x}_i) \tag{4.4}$$

allows us to recast Eq. (4.1) as the following matrix equation

$$\mathbf{\Phi}\dot{\mathbf{c}} = -i(\mathbf{H} - i\dot{\mathbf{\Phi}})\mathbf{c}, \tag{4.5}$$

where

$$\Phi_{ij} = \phi_j(\mathbf{x}_i) \tag{4.6a}$$

$$\begin{aligned}\dot{\Phi}_{ij} &= \sum_{k=1}^{N_d} \left.\frac{\partial \phi_j}{\partial t}\right|_{x_i^k} \\ &= \Bigg(\sum_{k=1}^{N_d} [2\alpha_{j_k} \dot{x}_{j_k} \Delta x_{(ji)_k} \\ &\qquad + i\dot{p}_{j_k} \Delta x_{(ji)_k} - i p_{j_k} \dot{x}_{j_k}] + \dot{\gamma}_j \Bigg) \Phi_{ij}\end{aligned} \tag{4.6b}$$

$$\begin{aligned}T_{ij} &= -\frac{1}{2m} \sum_{k=1}^{N_d} \left.\frac{\partial^2 \phi_j}{\partial x_k^2}\right|_{x_{i_k}} \\ &= -\frac{1}{2m} \sum_{k=1}^{N_d} \left[-2\alpha_{j_k} + \left(-2\alpha_{j_k} \Delta x_{(ji)_k} + i p_{j_k} \right)^2 \right] \Phi_{ij}\end{aligned} \tag{4.6c}$$

$$V_{ij} = V(\mathbf{x}_i) \Phi_{ij}. \tag{4.6d}$$

The explicit time-dependence of the basis set parameters has been dropped for clarity. The over dot indicates time derivatives calculated from the basis set equations of motion. The quantity $\Delta x_{(ji)_k} = (x_{j_k} - x_{i_k})$ is the separation between the centers of basis functions j and i in the kth degree of freedom. Φ is a discrete version of the overlap matrix. In this chapter the mass is the same for all degrees of freedom, hence independent of k, but we note this is not generally the case in molecular dynamics.

Propagating independent trajectories leads to a highly unstructured grid that resembles the framework of the QTM. We demonstrate the collocation form of the trajectory-guided TDSE is capable of describing quantum mechanical processes while avoiding the rigidity of a discrete variable representation grid and the numerical instabilities of the QTM.

Although Eq. (4.5) may be ill-conditioned, it can be readily solved for an accurate set of expansion coefficients $\{c_i\}$ through regularization methods for inverse problems.[69] We employ a singular value decomposition (SVD) with a threshold for removing small singular

values. Similar regularization methods are employed for the Gaussian-based methods with Gaussian test functions.[8, 11, 14, 15]

4.2.3 Equations of Motion

The equations of motion for the ith basis function are given by

$$\frac{\partial x_{i_k}}{\partial t} = \frac{\partial H}{\partial p_k} = \frac{p_{i_k}}{m} \tag{4.7a}$$

$$\frac{\partial p_{i_k}}{\partial t} = -\frac{\partial H}{\partial x_k} = -\left.\frac{\partial V(\mathbf{x})}{\partial x_k}\right|_{x_{i_k}} \tag{4.7b}$$

$$\frac{\partial \gamma_i}{\partial t} = -i\left(V(\mathbf{x}_i) + \sum_k^{N_d}[2\alpha_k - p_{i_k}^2]/2m\right). \tag{4.7c}$$

While these are easily recognized as the equations for a frozen Gaussian in the local harmonic approximation, they are also equivalent to the classical limit of the Bohmian DPM equations of motion. The relationship between Gaussian wave packet equations of motion and the DPM has been discussed recently by Zamstein and Tannor.[70] The equations of motion of a Gaussian wave packet can readily be related to the equations of motion for the spatial derivatives of the Bohmian wave function with complex action ansatz $\psi(x,t) = \exp(iS(x,t))$.

In the DPM, all of the initial trajectories correspond to the same initial Gaussian, but evolve into unique functions as local forces act on each trajectory. The final wave packet is then reconstructed by recognizing that each point represents the propagated amplitude of the initial state at a particular point. Eqs. (4.7a-4.7c) correspond to the trajectory initiated from the wave packet center. As in other Gaussian-based methods, we sample the centers of multiple Gaussians surrounding the initial wave packet in phase space. This differs from the DPM, where trajectories may be considered a swarm of Gaussians sampled from off-center points of the same initial state. Operating in a point wise perspective allows a clear connection to other guiding trajectories, including the propagation of Gaussians from points other than their phase space centers. Now, amplitudes may be assigned to the sampled

trajectories in the usual basis set fashion. Unlike most Gaussian-based methods, however, we maintain the point wise representation when calculating the quantum-mechanical coherence between trajectories. The matrix representation introduced in this chapter is means of properly treating coherence between arbitrary trajectories.

4.3 Applications

After a discussion of the computational details in Section 4.3.1 we present results for the Morse oscillator and the generalized Henon-Heiles potential in Section 4.3.2.

4.3.1 Computational Details

In all cases, the pseudospectral Gaussian results are compared to high-level quantum mechanical calculations. The sinc pseudospectral is used as a reference for the Morse potential and two-dimensional Henon-Heiles potential.[39, 51–56, 71–74] The exact propagation is performed using a straightforward application of the operator to the wave function $\psi(x, t + \Delta t) = \exp(-iH\Delta t)\psi(x, t)$. The four- and six-dimensional Henon-Heiles potentials are compared to MCTDH results.[22, 75, 76] Data from the benchmark study of Nest and Meyer is available freely online for comparison.[77] In addition we report calculations using the basis functions as the test functions, labeled as "Gaussian" calculations in this work. Data is presented using full analytical evaluation of the integrals (variational) and the BAT approximation (which has $\mathcal{O}(N_f)$ scaling with respect to potential energy evaluations).

In all cases, the initial state is taken to be an N_d-dimensional Gaussian. Both models are taken to represent adiabatic dynamics following instantaneous excitation from a harmonic ground state, implying the wave packet has $p_i = 0$ for i ranging from 1 to N_d. Additionally, the width of the initial wave packet is determined from the harmonic frequency of the potential ω where $\alpha = m\omega/2$, and the width of the basis functions is taken to be time-independent and equal to the width of the initial wave packet. The threshold to retain

singular values was set between 1×10^{-5} and 1×10^{-3} for all problems, where the precise choice was dictated by the potential and the equation type (i.e. collocation or Galerkin). The trajectory-based equations were propagated using a fourth order Runge-Kutta algorithm with a fixed time step of $dt = 0.1$ and $dt = 0.05$ for the Morse and Henon-Heiles potentials, respectively.

The initial position and momenta were sampled from a modified Wigner distribution for the initial Gaussian wave function.[78–81] In our calculations, we are able to achieve convergence using smaller basis sets if we compress the Wigner distribution sampling, producing more basis functions with significant overlap with the initial state. When the original Wigner distribution is used, convergence is much slower with respect to basis set size, suggesting the trajectories provide a poor basis for the quantum mechanics as the system evolves in time. Therefore, we introduce a compression parameter, β, similar to Shalashilin and Child, that narrows the sampled distribution. The standard deviations for position and momenta become $\beta\sigma_x$ and $\beta\sigma_p$, where a value of $\beta < 1$ narrows the sampling and $\beta = 1$ corresponds to standard Wigner sampling. The initial expansion coefficients for time-dependent problems are determined by projecting the basis onto the initial wave function, $c(t = 0) = \mathbf{\Phi}^{-1}\langle\delta(x - x_i)|\Psi\rangle$. The vector of elements $\langle\delta(x - x_i)|\Psi\rangle$, is the initial wave function evaluated at the basis function centers determined from sampling the Wigner distribution and $\mathbf{\Phi}^{-1}$ is the inverse of the discrete overlap matrix.

In both models, we calculate the autocorrelation function $C(t)$ and the spectrum via the Fourier transform of

$$C(t) = \langle\Psi(t = 0)|\Psi(t)\rangle. \tag{4.8}$$

However, since we begin with a real wave function, we can write[77, 82, 83]

$$C(t) = \langle\Psi(t = 0)|\Psi(t)\rangle = \langle\Psi^*(t/2)|\Psi(t/2)\rangle, \tag{4.9}$$

allowing the calculation of the correlation function from the wave function at half the time.

The spectrum is then calculated as

$$S(\omega) = \frac{1}{\pi}\mathrm{Re}\int_0^\infty e^{i\omega t}C(t)\cos(\pi t/2t_f)dt, \tag{4.10}$$

where the cosine function is a window function to suppress the Gibbs phenomenon when Fourier transforming a non-decaying signal and the spectrum is normalized such that $\int S(\omega)d\omega = 1$.[77]

4.3.2 Results

Time-independent Morse potential

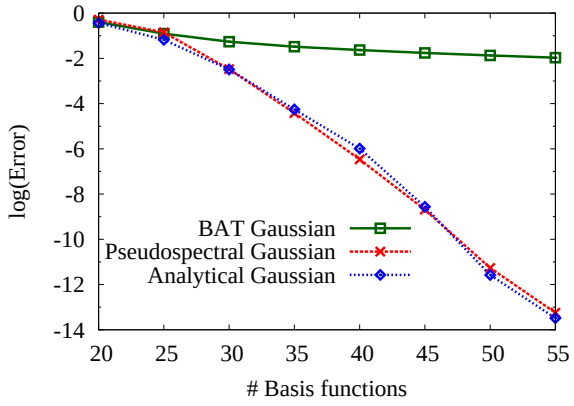

Figure 4.1: Error convergence calculated using the RMS of the ten lowest eigenvalues. Both the pseudospectral Gaussian and variational Gaussian methods exhibit exponential convergence. Although comparably accurate for small basis set sizes, the BAT error very slowly convergent.

Before considering the time-dependent dynamics, we calculate the vibrational energy levels of the Morse potential

$$V(x) = D\left(\exp(-2ax) - 2\exp(-ax)\right), \tag{4.11}$$

where $D = 10.25$a.u. and $a = 0.2209$ a.u.$^{-1}$ and the mass is 1 a.u.[84] The eigenvalue problem is solved on the interval $[-5.0, 15.0]$ with uniform spacing of the basis in Eq. (4.3) and p_i set

to zero.[32, 41, 85] We solve for the eigenvalues using a generalized eigenvalue solver.

To gauge the optimal accuracy of the Gaussian basis functions with both Gaussian and Dirac delta function test functions, we minimize the root-mean-square error of the first 10 energies with respect the width α of the Gaussian functions for each basis set size. Figure 4.1 plots the error convergence as a function of basis set size. There are at least two important features to the data. First, the pseudospectral and variational Gaussian methods are competitive in both accuracy and rate of convergence. This observation is consistent with the original findings of Yang and Peet.[41] We emphasize that the pseudospectral Gaussian calculation only required potential energy evaluations at the basis functions while the variational results are only available without numerical integration because the exponential form of the potential is analytically integrable. Second, the BAT approximation produces a poor representation of the Hamiltonian. Convergence is extremely slow even with the optimal α values computed for each basis set size. Applications of Gaussian collocation to time-independent multi-dimensional examples may be found in the original work of Yang and Peet and more recently in the work of Carrington and co-workers.[43, 45, 64, 66]

In all cases, the optimal width of the basis function narrows (larger alpha) as the basis set increases. This is consistent with the width selection process of Hamilton and Light in Ref. [32]. The optimal widths using twenty basis functions for pseudospectral Gaussian, analytical, and BAT, are 0.21, 0.78 and 1.22, respectively. The optimal widths for fifty-five basis functions are 1.25, 1.5, 11.45. The broader basis functions for collocation is consistent with the observations of Yang and Peet in Ref. [41].

Time-dependent Morse potential

As an evaluation of the method's ability to describe quantum-mechanical coherence, we investigate the time evolution of wave packet in a Morse potential.[84] The potential is given by Eq. (4.11). The initial wave packet is selected to have a width of $\alpha = 1/2$ a.u.$^{-2}$ and a center of $x_c = 9.432$ a.u. Both the wave packet and potential parameters are originally

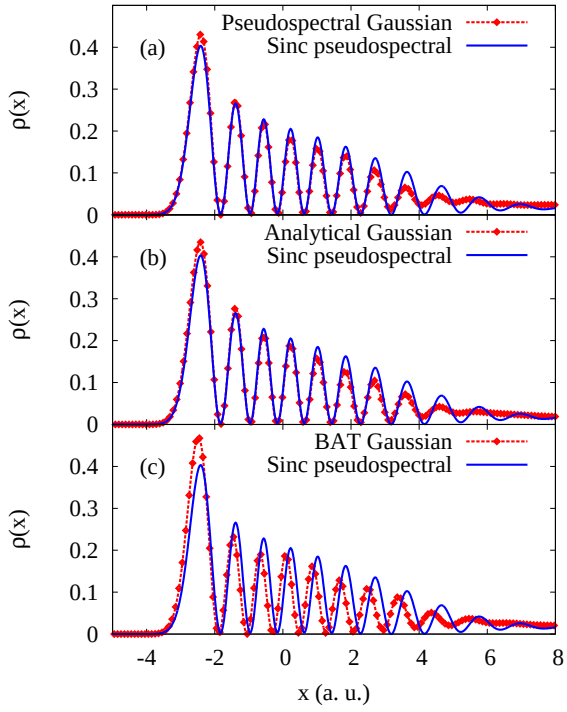

Figure 4.2: The density at $t = 6$ for the pseudospectral, analytical, and BAT Gaussian dynamics. Both the pseudospectral and analytical Gaussian methods capture the proper coherence in the density. The BAT density captures the peaks but is displaced slightly from the pseudospectral results.

from Ref. [86] although they have been used to evaluate semiclassical methods in other publications as well.[36, 70]

First, we consider the density at $t = 6$ a.u., when the wave packet is in the process of reflecting from the steep repulsive wall of the Morse potential. Fig. 4.2 compares the densities from the pseudospectral, analytical, and BAT Gaussian methods with the sinc pseudospectral method at $t = 6$ a.u. Each Gaussian method uses 400 basis functions (trajectories) with no sampling compression $\beta = 1$. In all three cases the Gaussian dynamics reflect the highly oscillatory density caused by significant quantum-mechanical coherence; however, the BAT approximation is out of phase slightly with respect to the exact density.

We consider longer time dynamics in Fig. 4.3 where we plot the real part of $C(t)$ at $t = 50$ a.u. Both the pseudospectral Gaussian and the analytical Gaussian methods are in excellent agreement with the exact results throughout the propagation. Interestingly, the BAT method

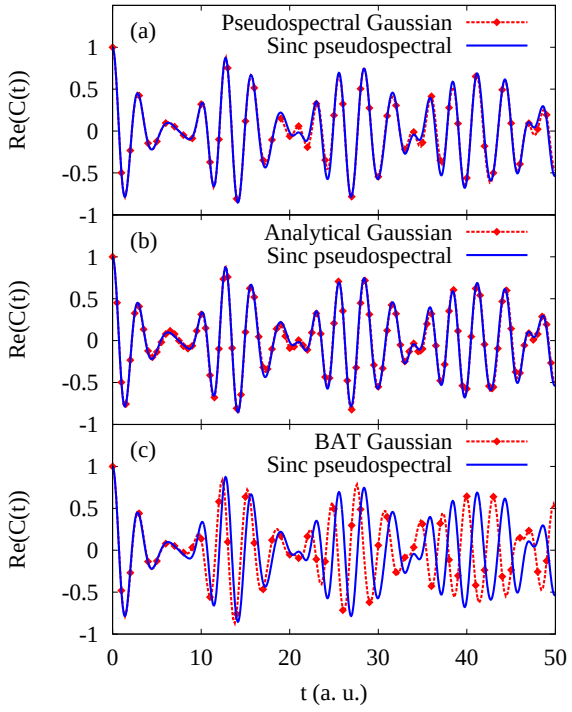

Figure 4.3: $C(t)$ for the pseudospectral, analytical, and BAT Gaussian dynamics up to $t = 50$. Both the pseudospectral and analytical Gaussian calculations are in excellent agreement with the exact results. Interestingly, the BAT's $C(t)$ slowly becomes out of phase with the exact result. The first departure is between $t = 5$ and $t = 10$, the point of reflection against the steep wall of the Morse potential. $C(t)$ becomes more out of phase for each recurrence in the correlation function.

struggles with the strong coherence. Although the amplitude remains reasonable, the BAT's $C(t)$ grows increasingly out of phase with the exact result. Neither reducing the time step nor increasing basis set size improves the BAT's correlation function.

The Morse potential, although one-dimensional, is a nontrivial test of quantum-mechanical coherence for trajectory-based methods. The pseudospectral Gaussian and the analytical Gaussian methods give similarly accurate results. Yet, unlike the analytical Gaussian method, the pseudospectral sampling does not require a closed form for the potential to avoid computationally costly numerical integration. Moreover, we demonstrate that an approximation within the analytical Gaussian method of comparable cost, the BAT, is incapable of accurately describing the highly oscillatory behavior of this Morse model.

Henon-Heiles potential

To evaluate the validity of the results from the Morse potential when investigating higher-dimensional systems, we study an N-dimensional generalization of the Henon-Heiles potential.[87] The model, which has been used extensively to evaluate the performance of semi-classical and quantum mechanical methods.[4, 5, 12, 77, 80, 88–91] The model offers a convenient avenue for testing, on an anharmonic non-separable potential, a method's performance a with dimensionality. We adopt the form of the potential used in many other papers[12, 77, 80, 89–91]

$$V(x) = \frac{1}{2}\sum_{i=1}^{N_d} x_i^2 + \lambda \sum_{i=1}^{N_d-1}\left(x_i^2 x_{i+1} - \frac{1}{3}x_{i+1}^3\right) \tag{4.12}$$

with $\lambda = 0.111803$. The initial wave packet width is set to the harmonic frequency of the potential $\alpha_i = 1/2$. Every coordinate initially has zero momentum $p_i = 0$ and a displacement of two $x_i = 2$ for $i = 1, 2, \ldots, N_d$. All calculations begin with 500 Gaussian basis functions unless otherwise noted. Since every coordinate is displaced, the energy for the wave packet grows with dimensionality. Similar to the Gaussian-MCTDH study, dissociated trajectories lead to numerical stabilities in the integration.[12] Therefore, we discard trajectories for which the center for any coordinate exceeds 12 a.u. from the origin. Typically, by this criterion, 50-60% of the basis sets and their trajectories in the pseudospectral Gaussian, analytical Gaussian, and BAT Gaussian methods are discarded by the end of the calculation. Although the amplitudes of these discarded basis functions are neglected, dissociated trajectories do not overlap with the initial state and therefore do not affect the calculation of the correlation function.

First, we consider the two-dimensional model. The generalized Henon-Heiles model's dynamics are more complicated for lower dimensions.[77] Fig. 4.4 compares the $C(t)$ following propagation to $t = 25$ a.u. which reveals important characteristics of the methods. Similar to the Morse potential, both the pseudospectral Gaussian and the analytical Gaussian methods capture the recurrences and the smaller amplitude interference that grows as the wave packet

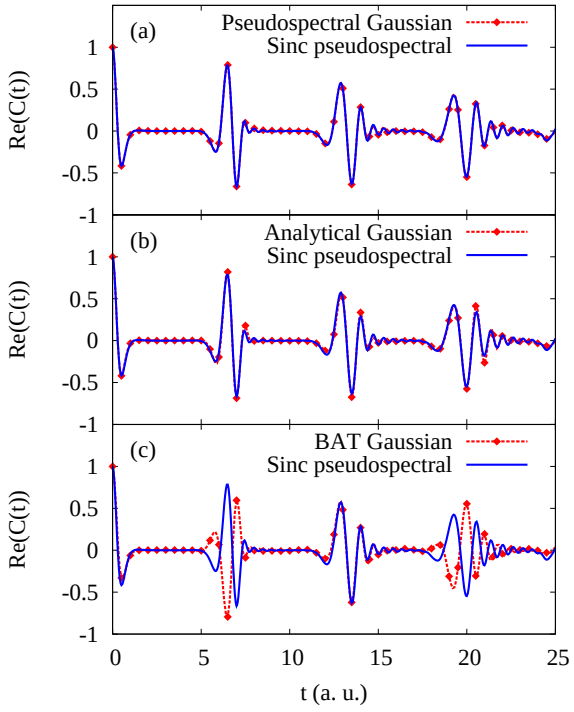

Figure 4.4: $C(t)$ for the two-dimensional Henon-Heiles model for 25 time units. The pseudospectral Gaussian and analytical results are nearly indistinguishable from the sinc pseudospectral method. The BAT maintains the qualitative structure of $C(t)$ but fails to maintain the proper phase for the first and third recurrence..

spreads. While the BAT's $C(t)$ is out of phase for the first and third recurrences, the second recurrence is reproduced very well. While it is not clear what causes the error and how general it may be, the phase shift is consistent with results for the Morse potential. It appears that the BAT breaks down when the quantum-mechanical interference becomes strong.

Second, we consider the four- and six-dimensional models. In the four-dimensional case, rather than testing the short-time dynamics using a small basis set, we seek to reproduce the complicated spectrum obtained from longer propagation. The spectrum $S(\omega)$ at $t =$ 200 a.u. following propagation for 100 a.u. of time using 1,500 trajectories and $\beta = 0.6$ is presented in Fig. 4.5. Although the pseudospectral Gaussian spectrum is noisier than the MCTDH, the agreement in peak location and intensity is generally very good. In the lower panel of Fig. 4.5 the higher-energy portion of the spectrum is expanded, revealing the significant anharmonic splitting for these states.

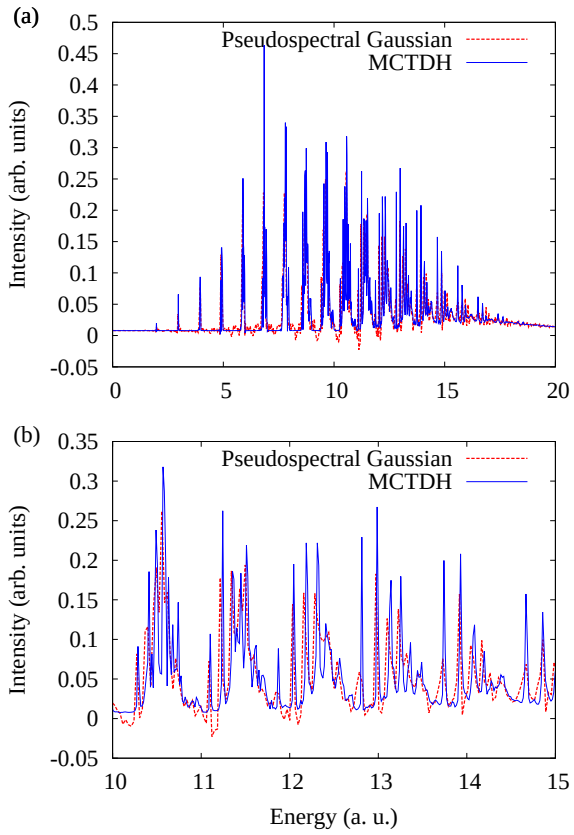

Figure 4.5: The spectrum corresponding to wave packet propagation in the 4-D model for 200 time units using the pseudospectral Gaussian method. The top panel, (a), presents the entire spectrum while the lower panel, (b), focuses on splitting in the higher-energy peaks. While the pseudospectral Gaussian spectrum is noisy, it still captures many of the important features including the splitting in higher-energy peaks. 1,500 trajectories were used with $\beta = 0.6$.

The six-dimensional model is considerably simpler than the two- and four-dimensional cases. In higher dimensions $C(t)$ decays much faster and there is less coherence between the degrees of freedom.[77] As a result, the spectrum is calculated for the six-dimensional model following propagation to $t = 50$ a.u. using 500 trajectories and $\beta = 0.3$. These conditions are sufficient to obtain excellent agreement between the pseudospectral and analytical Gaussian methods (Fig 4.6). Once again, there is more noise in the baseline of the Gaussian methods than the MCTDH method, but the energy bands from both methods are nearly indistinguishable. The BAT method produces a spectrum that nearly resembles the MCTDH result but is shifted slightly in energy. As seen in the one- and two-dimensional models, the agree-

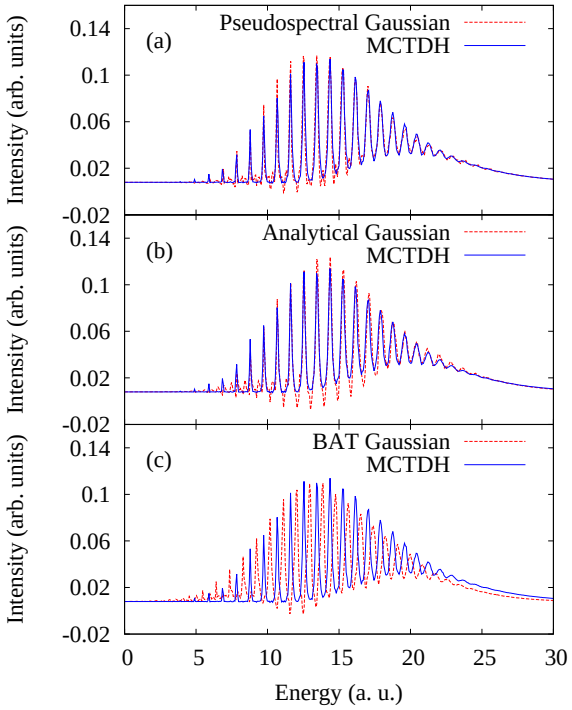

Figure 4.6: The spectra for the 6-D Henon-Heiles potential. 500 trajectories were used and $\beta = 0.3$. The pseudospectral Gaussian spectrum is nearly indistinguishable from the MCTDH results. The noise along the baseline reflects the slightly poorer quality of the time correlation function, but overall the agreement is excellent. Once again, the BAT data bears some resemblance to the exact result but the energies are shifted from the exact results.

ment is not improved by using more basis functions or a smaller time step. The persistent inability to maintain wave packet phase in higher dimensions suggests the error is not merely an artifact of the low-dimensional models. We do note that the model problems presented here are considerably more difficult than many scattering or dissociative processes for which the BAT approximation may be more accurate.

4.4 Discussion and Conclusions

Quantum molecular dynamics must be able to generate an accurate representation of the potential energy surface from a minimal number of electronic structure calculations for computational efficiency. In this chapter we have presented a trajectory-based pseudospectral Gaussian quantum molecular dynamics method that requires only $\mathcal{O}(N)$ sampling of the

potential energy surface where N is the number of Gaussian basis functions. In contrast to other approaches which use the Gaussian basis functions as test functions, the pseudospectral Gaussian method tests the time-independent Schrödinger equation with Dirac delta functions located at the centers of the Gaussian basis functions. While the selection of Gaussian basis functions as test functions requires numerical integration to represent the potential, the selection of Dirac delta functions simplifies the numerical integration, scaling as $O(N^2)$, to N evaluations of the potential energy surface, scaling as $\mathcal{O}(N)$. The pseudospectral Gaussian molecular dynamics method provides a new tool for performing the quantum dynamics more efficiently for molecular systems with significant strong electron correlation. It can be easily interfaced with electronic structure methods including wave function and reduced density matrix methods.

Applications to diatomic vibrations modeled by the Morse potential and a generalized Henon-Heiles model demonstrate the quantitative accuracy of pseudospectral sampling of a time-dependent basis. Despite the significant reduction in information required to propagate the wave packet,the pseudospectral Gaussian method is capable of coherent quantum-mechanical propagation as accurate as variational calculations. While, for time-independent basis sets, pseudospectral (collocation) methods historically perform comparably to spectral (Galerkin), the method here employs a time-dependent unstructured grid defined by the Gaussian trajectories.. Nevertheless, we demonstrate that pseudospectral sampling of the time-dependent basis set does not comprise the accuracy of variational calculations and yet does not require expensive numerical integrations involving the potential energy surface.

While pseudospectral sampling of the Gaussian basis set introduces a new approach to Gaussian wave packet dynamics, it is important to realize that the collocation scheme presented here is compatible with much of the existing machinery for trajectory-based Gaussian methods. Pseudospectral Gaussian dynamics may easily be incorporated in an AIMS-like non-adiabatic method[6, 8, 16, 58] or merged with the coupled coherent states method where considerable effort has been put forth to improve initial condition selection and trajectory

sampling.[34, 36, 80, 90] The method is also compatible with other recent Gaussian-based methods such as basis expansion leaping[14] and the basis set generation method of Saller and Habershon.[15]

In this chapter, we have introduced a novel numerical framework for trajectory-based Gaussian methods that employs pseudospectral sampling of the basis set. We demonstrate that sampling time-dependent basis functions with Dirac delta functions produces a method capable of stable and accurate quantum dynamics. Furthermore, we propose that the $\mathcal{O}(N)$ potential energy sampling inherited from pseudospectral sampling makes the method a good candidate for on-the-fly quantum molecular dynamics where electronic structure calculations are computationally expensive. Rather than using the basis functions as test functions, we take heed of Boyd's advice regarding the advantage of pseudospectral (collocation) methods over spectral (Galerkin) methods, "the reason is simply that it is easier to evaluate a function than it is to integrate it."[38] This approach has, in our opinion, been underutilized thus far in time-dependent basis methods, and its further development has the potential to open new problems in chemical physics to an accurate treatment by quantum dynamics.

4.5 References

[1] E. J. Heller, J. Chem. Phys. **62**, 1544 (1975).

[2] E. J. Heller, J. Chem. Phys. **75**, 2923 (1981).

[3] S. Sawada, R. Heather, B. Jackson, and H. Metiu, J. Chem. Phys. **83**, 3009 (1985).

[4] D. Huber and E. J. Heller, J. Chem. Phys. **89**, 4752 (1988).

[5] D. Huber, S. Ling, D. G. Imre, and E. J. Heller, J. Chem. Phys. **90**, 7317 (1989).

[6] T. J. Martínez, M. Ben-Nun, and R. D. Levine, J. Phys. Chem. **100**, 7884 (1996).

[7] T. J. Martínez, M. Ben-Nun, and G. Ashkenazi, J. Chem. Phys. **104**, 2847 (1996).

[8] M. Ben-Nun and T. J. Martínez, J. Chem. Phys. **108**, 7244 (1998).

[9] Y. Wu and V. S. Batista, J. Chem. Phys. **118**, 6720 (2003).

[10] Y. Wu and V. S. Batista, J. Chem. Phys. **121**, 1676 (2004).

[11] I. Burghardt, M. Nest, and G. A. Worth, J. Chem. Phys. **119**, 5364 (2003).

[12] G. A. Worth and I. Burghardt, Chem. Phys. Lett. **368**, 502 (2003).

[13] S. Habershon, J. Chem. Phys. **136**, (2012).

[14] W. Koch and T. J. Frankcombe, Phys. Rev. Lett. **110**, 263202 (2013).

[15] M. A. C. Saller and S. Habershon, J. Chem. Theory Comput. **11**, 8 (2015).

[16] M. Ben-Nun and T. J. Martínez, Chem. Phys. Lett. **298**, 57 (1998).

[17] M. Ben-Nun and T. J. Martínez, J. Chem. Phys. **110**, 4134 (1999).

[18] M. Ben-Nun, J. Quenneville, and T. J. Martínez, J. Phys. Chem. A **104**, 5161 (2000).

[19] M. Ben-Nun and T. J. Martínez, Adv. Chem. Phys. **121**, 439 (2002).

[20] S. S. Iyengar and J. Jakowski, J. Chem. Phys. **122** (2005).

[21] X. Li and S. S. Iyengar, J. Chem. Phys. **133**, 184105 (2010).

[22] M. Beck, A. Jäckle, G. Worth, and H.-D. Meyer, Phys. Rep. **324**, 1 (2000).

[23] C. Leveque, A. Komainda, R. Taieb, and H. Koppel, J. Chem. Phys. **138**, 044320 (2013).

[24] I. Tavernelli, Phys. Rev. A **87**, 042501 (2013).

[25] D. V. Makhov, W. J. Glover, T. J. Martínez, and D. V. Shalashilin, J. Chem. Phys. **141**, 054110 (2014).

[26] B. Lasorne, G. Worth, and M. Robb, in *Molecular Quantum Dynamics*, edited by F. Gatti (Springer Berlin Heidelberg, 2014), pp. 181–211.

[27] B. Roos, Adv. Chem. Phys. **69**, 399 (1987).

[28] D. A. Mazziotti, Adv. Chem. Phys. **134**, 19 (2007).

[29] T. Tsuchimochi and G. E. Scuseria, J. Chem. Phys. **131**, 121102 (2009).

[30] T. Yanai, Y. Kurashige, E. Neuscamman, and G. K.-L. Chan, J. Chem. Phys. **132**, 024105 (2010).

[31] D. A. Mazziotti, Chem. Rev. **112**, 244 (2012).

[32] I. P. Hamilton and J. C. Light, J. Chem. Phys. **84**, 306 (1986).

[33] B. Poirier and J. C. Light, J. Chem. Phys. **113**, 211 (2000).

[34] D. V. Shalashilin and M. S. Child, J. Chem. Phys. **113**, 10028 (2000).

[35] S. Garashchuk and J. C. Light, J. Chem. Phys. **114**, 3929 (2001).

[36] D. V. Shalashilin and M. S. Child, Chem. Phys. **304**, 103 (2004).

[37] B. Hartke, Phys. Chem. Chem. Phys. **8**, 3627 (2006).

[38] J. Boyd, *Chebyshev and Fourier Spectral Methods: Second Revised Edition*, Dover Books on Mathematics (Dover Publications, 2001).

[39] J. Lill, G. Parker, and J. Light, Chem. Phys. Lett. **89**, 483 (1982).

[40] D. Kosloff and R. Kosloff, J. Comput. Phys. **52**, 35 (1983).

[41] W. Yang and A. C. Peet, Chem. Phys. Lett. **153**, 98 (1988).

[42] W. Yang, A. C. Peet, and W. H. Miller, J. Chem. Phys. **91**, 7537 (1989).

[43] A. C. Peet and W. Yang, J. Chem. Phys. **91**, 6598 (1989).

[44] A. C. Peet and W. Yang, J. Chem. Phys. **90**, 1746 (1989).

[45] W. Yang and A. C. Peet, J. Chem. Phys. **92**, 522 (1990).

[46] M. Dehghan and A. Shokri, Comput. Math. Appl. **54**, 136 (2007).

[47] J. Sielk, H. F. von Horsten, F. Kruger, R. Schneider, and B. Hartke, Phys. Chem. Chem. Phys. **11**, 463 (2009).

[48] A. Shimshovitz and D. J. Tannor, J. Chem. Phys. **137**, 101103 (2012).

[49] A. Shimshovitz and D. J. Tannor, Phys. Rev. Lett. **109**, 070402 (2012).

[50] K. Kormann and E. Larsson, SIAM J. Sci. Comput. **35**, A2832 (2013).

[51] S. A. Orszag, Phys. Fluids **12**, 250 (1969).

[52] D. Gottlieb and S. Orszag, *Numerical Analysis of Spectral Methods: Theory and Applications* (SIAM, 1977).

[53] D. Furnaro, in *Polynomial Approximation of Differential Equations* (Springer-Verlag Heidelberg, 1992), vol. 8 of *Lecture Notes in Physics*.

[54] B. Fornberg, *A Practical Guide to Pseudospectral Methods* (Cambridge University Press, 1998).

[55] C. Canuto, M. Y. Hussaini, A. Quarteroni, and T. Zang, *Spectral Methods: Fundamentals in Single Domains* (Springer-Verlag Berlin Heidelberg, 2006).

[56] J. S. Hesthaven, S. Gottlieb, and D. Gottlieb, *Spectral methods for time-dependent problems* (Cambridge University Press, 2007).

[57] D. Tannor, *Introduction to Quantum Mechanics: A Time-dependent Perspective* (University Science Books, 2007).

[58] T. J. Martínez, M. Ben-Nun, and R. D. Levine, J. Phys. Chem. A **101**, 6389 (1997).

[59] C. L. Lopreore and R. E. Wyatt, Phys. Rev. Lett. **82**, 5190 (1999).

[60] R. Wyatt and C. Trahan, *Quantum Dynamics with Trajectories: Introduction to Quantum Hydrodynamics*, Interdisciplinary applied mathematics (Springer, 2006).

[61] Y. Goldfarb, I. Degani, and D. J. Tannor, J. Chem. Phys. **125**, 231103 (2006).

[62] G. Albareda, H. Appel, I. Franco, A. Abedi, and A. Rubio, Phys. Rev. Lett. **113**, 083003 (2014).

[63] G. Albareda, J. M. Bofill, I. Tavernelli, F. Huarte-Larrañaga, F. Illas, and A. Rubio, J. Phys. Chem. Lett. **6**, 1529 (2015).

[64] S. Manzhos and T. Carrington Jr., Can. J. Chem. **87**, 864 (2009).

[65] S. Manzhos, T. Carrington Jr., and K. Yamashita, Surf. Sci. **605**, 616 (2011).

[66] S. Manzhos, K. Yamashita, and T. Carrington Jr., Chem. Phys. Lett. **511**, 434 (2011).

[67] K. Saita and D. V. Shalashilin, J. Chem. Phys. **137**, 22A506 (2012).

[68] D. Makhov, K. Saita, T. J. Martínez, and D. Shalashilin, Phys. Chem. Chem. Phys. **17**, 3316 (2014).

[69] P. Hansen, *Discrete Inverse Problems: Insight and Algorithms*, Fundamentals of Algorithms (SIAM, 2010).

[70] N. Zamstein and D. J. Tannor, J. Chem. Phys. **140**, 041105 (2014).

[71] D. T. Colbert and W. H. Miller, J. Chem. Phys. **96**, 1982 (1992).

[72] J. C. Light and T. Carrington Jr., Adv. Chem. Phys. **114** (2000).

[73] D. A. Mazziotti, Chem. Phys. Lett. **299**, 473 (1999).

[74] D. A. Mazziotti, J. Chem. Phys. **117**, 2455 (2002).

[75] H.-D. Meyer, U. Manthe, and L. Cederbaum, Chem. Phys. Lett. **165**, 73 (1990).

[76] U. Manthe, H. Meyer, and L. S. Cederbaum, J. Chem. Phys. **97**, 3199 (1992).

[77] M. Nest and H.-D. Meyer, J. Chem. Phys. **117**, 10499 (2002).

[78] E. Wigner, Phys. Rev. **40**, 749 (1932).

[79] E. J. Heller, J. Chem. Phys. **65**, 1289 (1976).

[80] D. V. Shalashilin and M. S. Child, J. Chem. Phys. **128**, 054102 (2008).

[81] D. V. Shalashilin, J. Chem. Phys. **130**, 244101 (2009).

[82] V. Engel, Chem. Phys. Lett. **189**, 76 (1992).

[83] U. Manthe, H. Meyer, and L. S. Cederbaum, J. Chem. Phys. **97**, 9062 (1992).

[84] W. H. Miller, J. Chem. Phys. **136**, 210901 (2012).

[85] M. J. Davis and E. J. Heller, J. Chem. Phys. **71**, 3383 (1979).

[86] D. Huber and E. J. Heller, J. Chem. Phys. **87**, 5302 (1987).

[87] M. Henon and C. Heiles, Astron. J. **69**, 73 (1964).

[88] A. R. Walton and D. E. Manolopoulos, Mol. Phys. **87**, 961 (1996).

[89] M. L. Brewer, J. Chem. Phys. **111**, 6168 (1999).

[90] D. V. Shalashilin and M. S. Child, J. Chem. Phys. **115**, 5367 (2001).

[91] O. Vendrell and H.-D. Meyer, J. Chem. Phys. **134**, 044135 (2011).

CHAPTER 5

NONADIABATIC PSEUDOSPECTRAL GAUSSIAN DYNAMICS

This chapter contains work that is in preparation for submission for publication.

5.1 Introduction

For the vast majority of molecular dynamics, the Born-Oppenheimer approximation is valid and the nuclear evolution may be described by a single electronic potential energy surface. However, nonadiabatic dynamics, or cases when the Born-Oppenheimer approximation breaks down, characterize many important reactions in chemistry, from charge transfer in materials to photo-induced biological processes.[1–5] Unfortunately, the *ab initio* description of nonadiabatic chemical processes is still a significant challenge for computation because of the accuracy and efficiency required for both the quantum molecular dynamics and the molecular electronic structure.[3, 4, 6–17] Electronic structure calculations for nonadiabatic dynamics require accurate excited electronic states and the ability to provide a balanced description of strong correlation.[18–23] Introducing a time-dependent (trajectory-guided) basis set circumvents the exponential scaling of traditional grid methods and is compatible with the direct determination of the potential energy surface from electronic structure calculations. In this work, we implement the nonadiabatic extension of a recently introduced trajectory-guided Gaussian basis set for quantum molecular dynamics called pseudospectral Gaussian dynamics. The most important advantage of pseudospectral Gaussian dynamics is the ability to match the accuracy of analytical potential energy integration while requiring no *a priori* knowledge of the potential energy surface and only requiring $\mathcal{O}(N)$ sampling, where N is the number of basis functions, of the potential energy surface.

Two particularly important components of a nonadiabatic trajectory-guided basis set method pertaining to this work are 1) the coupling between trajectories or expression of the

Hamiltonian and 2) the equations of motion for basis functions. This chapter focuses on an accurate and efficient way to couple trajectories in nonadiabatic dynamics. In Gaussian based methods, the basis set is typically tested using the complex conjugate of the basis functions.[24–30] While this leads to a Hermitian Hamiltonian, it requires integral evaluation over all space, a nontrivial task for the potential energy. Generally, approximations such as the local harmonic approximation (LHA), saddle point approximation (SPA) and the bra-ket averaged Taylor expansion (BAT) are introduced to generate the Hamiltonian.[6, 12, 14, 16, 25, 31–34] However, these approximations often require additional electronic structure calculations and rely on the locality of the Gaussian basis functions to ensure accuracy.

Pseudospectral Gaussian dynamics departs from typical Gaussian-based methods by choosing the Dirac delta function as the test function.[35–43] The delta function test function reduces the integral evaluation to function evaluation.[38, 40–45] The Hamiltonian may now be expressed exactly without approximation to the potential energy and the $\mathcal{O}(N)$ scaling means only the electronic structure information for the classical trajectories is required to incorporate the quantum dynamics. The Dirac delta function test function is also a distinguishing feature of the pseudospectral method.[35, 46–52]

Having introduced a prescription to efficiently represent the Hamiltonian, the time-dependence of the basis functions needs to be prescribed. While classical equations of motion are often sufficient for single-surface dynamics, nonadiabatic population transfer precludes the straightforward definition of a single, classical force. In this work, we use Ehrenfest trajectories to propagate the basis functions. While Ehrenfest trajectories are suitable for some of the applications we present, it is well known that they provide a qualitatively incorrect description of nonadiabatic processes when the gradients of the multiple potential energy surfaces differ significantly. The consequence is that many more trajectories are required for convergence than would likely be needed if an improved selection of trajectories was made. The ab initio multiple spawning (AIMS) algorithm of Martínez and co-workers is a very effective approach to minimizing basis set size and would be expected to accelerate conver-

gence. Nevertheless, we observe well-behaved convergence to the exact solution for one- and two-dimensional examples using Ehrenfest trajectories.

The discretized grid of nonadiabatic pseudospectral Gaussian dynamics places the method at the intersection of independent trajectory, Gaussian basis set expansion, and nonadiabatic Bohmian methods. While we adopt a basis of independently propagated Gaussians as in AIMS, the numerical framework resembles that of a Bohmian grid where each trajectory corresponds to a discrete point in space with an associated amplitude of the wave function.[53–58] By associating with each Bohmian trajectory a Gaussian basis function, we are able to build a matrix form of the time-dependent Schrödinger equation that circumvents the challenging spacial derivatives and nodal instabilities in Bohmian mechanics.[53–58] Interestingly, many of the methods to describe decoherence in FSSH also invoke a Gaussian form for individual trajectories.[59–68] Introducing the Gaussian overlap allows the straightforward calculation of overlap decoherence criteria and a route to an improved description of quantum mechanical behavior in FSSH. Since the pseudospectral Gaussian method, without approximation, requires only the information used in FSSH propagation, the construction of the full Hamiltonian may be viewed as a means of coupling all trajectories simultaneously. The cost is the requirement to solve a system of equations $Ax = b$ at each time step. However, if solving the linear system of equations provides converged results using many fewer trajectories, the calculation time may be dominated by electronic structure calculations in on-the-fly applications.

The discretization here should not be confused with the phase space discretization discussed in some coherent state methods.[26–28] In those cases, position and momenta are discretized to approximate the complete set of coherent states, but the basis set is still tested with the basis functions requiring the approximation of potential integrals. In this chapter, we also begin with a discretized basis set in phase space, but we then project the basis onto discrete points in space. This step discretizes the wave function in addition to the basis set. Although this approach is very common in in the broader community, trajectory-

guided Gaussian methods are predominantly solved in the functional space of the basis rather than projected onto spatial points.

In the present chapter, we build upon our recent work applying pseudospectral Gaussian method to a single Born-Oppenheimer potential energy surface by studying nonadiabatic model systems in the diabatic representation. First, we review the equations of the pseudospectral Gaussian method including the Hamiltonian elements required to couple surfaces and equations of motion for the basis functions. The first application uses a model of coupled Morse potentials to study photo induced dynamics. We consider a set of three-surface photodissociation models and a two-surface case of bound excitation leading to anharmonic oscillation.[69, 70] The third case studied is a two-dimensional model corresponding to vibrational dynamics in a collinear triatomic molecule.[71, 72] Collectively, these model systems allow us to test many important features including multiple crossings through regions of coupling, spatial separation of surface densities, and intra-surface coupling effects. Not only is the pseudospectral Gaussian method able to accurately describe population dynamics, it also allows for accurate wave packet reconstruction after long propagation times.

5.2 Theory

The pseudospectral Gaussian method is reviewed with a discussion of the test functions, basis functions and associated equations of motion in Section 5.2.1. In Section 5.2.2 we present the matrix form of the working equations is for nonadiabatic dynamics in the diabatic and adiabatic representation.

5.2.1 Test and Basis Functions

Testing the time-dependent Schrödinger equation with the N_f test functions χ_i yields

$$\left\langle \chi_i(t) \left| i\frac{d}{dt} - \hat{H} \right| \Psi(t) \right\rangle = 0. \tag{5.1}$$

We may expand the total wave function using the Born-Huang expansion in the basis of orthonormal electronic states[73],

$$\Psi(\mathbf{r}, \mathbf{x}, t) = \sum_{I}^{\infty} C^I(t)\Omega^I(\mathbf{r}; \mathbf{x})\Phi^I(\mathbf{x}, t), \tag{5.2}$$

where $\Omega(\mathbf{r}; \mathbf{x})$ is a complete set of orthonormal electronic wave functions that depend parametrically on nuclear coordinates and $\Phi^I(\mathbf{r}, t)$ is the time-dependent nuclear wave function for the I-th electronic state. Throughout the chapter r denotes the fast (electronic) coordinates and x denotes the slow (nuclear) coordinates. Superscripts and capital letters denote electronic states while subscripts and lower case letters denote primitive Gaussians in the nuclear wave function expansion for a given electronic state.

The wave function for the I-th electronic state can be expanded in terms of N_f basis functions ϕ_i,

$$|\Phi^I(\mathbf{x}, t)\rangle = \sum_{i}^{N_f} c_i(t)\phi_i(\mathbf{x}, t). \tag{5.3}$$

If both the basis and test functions are chosen to be Gaussian functions, then the evaluation of the potential requires numerical integration which, without approximation, scales as $\mathcal{O}(N_f^2)$. However, if we choose the test functions to be Dirac delta functions, located at the centers of the Gaussian basis functions, then the evaluation of the potential scales as $\mathcal{O}(N_f)$. The Gaussian functions are chosen to be time-dependent, moving according to Hamilton's equations of motion. For clarity, we introduce $D_j^I = C^I c_j$ where both the electronic state amplitude and single state expansion coefficient have been absorbed into a single expansion coefficient.

Each basis function, for a problem in N_d-dimensions, is given as a product of one-

dimensional functions

$$\phi_i(\mathbf{x}, \mathbf{t}; \alpha_i, \mathbf{x}_i(t), \mathbf{p}_i(t), \gamma_i(t)) = \exp(\gamma_i) \prod_{k=1}^{N_d} \exp(-\alpha_{i_k}(\Delta x_{i_k})^2 + i p_{i_k}(\Delta x_{i_k})), \tag{5.4}$$

where $\Delta x_{i_k} = (x_k - x_{i_k})$ and the width is time-independent (frozen Gaussians).[74] The parameter γ_i is complex, accounting for phase and normalization and determined by the local harmonic approximation.[31] N_f is the basis set size while N_d is the number of degrees of freedom in the system. Therefore, $\mathbf{x}_i$ and $\mathbf{p}_i$ represent the N_d-dimensional vectors corresponding to the time-dependent basis function position and momentum centers for the i-th basis function.

The equations of motion for the ith basis function are given by

$$\frac{\partial x_{i_k}}{\partial t} = \frac{p_{i_k}}{m} \tag{5.5a}$$

$$\frac{\partial p_{i_k}}{\partial t} = -\left.\frac{\partial V_{\mathrm{Ehr}}(\mathbf{x})}{\partial x_k}\right|_{x_{i_k}} \tag{5.5b}$$

$$\frac{\partial \gamma_i}{\partial t} = -i\left(V^{\mathrm{Ehr}}(\mathbf{x}_i) + \sum_k^{N_d}[2\alpha_k - p_{i_k}^2]/2m\right). \tag{5.5c}$$

The trajectories are by the Ehrenfest potential energy, defined by the state averaged Hamiltonian,

$$V^{\mathrm{Ehr}}(\mathbf{x}_i) = \frac{|D_i^1|^2 V_1(\mathbf{x}_i) + |D_i^2|^2 V_2(\mathbf{x}_i) + 2\mathrm{Re}(D_i^{1*} D_i^2 V_{12}(\mathbf{x}_i))}{|D_i^1|^2 + |D_i^2|^2}, \tag{5.6}$$

which has been written explicitly for basis function i in a two level system.[75, 76]

5.2.2 Matrix Equations and their Solution

Assigning the N_d-dimensional Dirac delta function to the test function

$$|\chi_i\rangle = \delta(\mathbf{x} - \mathbf{x}_i) \tag{5.7}$$

allows us to recast Eq. (5.1) as the following matrix equation

$$\dot{\mathbf{D}}^I = -i\mathbf{\Phi}^{-1}\left(\mathbf{H}^{II} - i\dot{\mathbf{\Phi}}\right)\mathbf{D}^I + \sum_{J,I\neq J}\mathbf{H}^{IJ}\mathbf{D}^J, \tag{5.8}$$

where the first term on the RHS of Eq. (5.8) accounts for intra surface coupling and the second term, $I \neq J$, accounts for inter surface coupling. The explicit matrix elements are

$$\Phi_{ij} = \phi_j(\mathbf{x}_i) \tag{5.9}$$

$$\frac{\partial \Phi_{ij}}{\partial t} = \sum_{k=1}^{N_d}\left.\frac{\partial \phi_j}{\partial t}\right|_{\mathbf{x}_i} \tag{5.10}$$

$$H_{ij}^{II} = -\sum_{k=1}^{N_d}\left.\frac{1}{2m_k}\frac{\partial^2\phi_j}{\partial x_k^2}\right|_{\mathbf{x}_i} + V^{II}(\mathbf{x}_i)\phi_j(\mathbf{x}_i) \tag{5.11}$$

$$H_{ij}^{IJ} = V^{IJ}(\mathbf{x}_i)\phi_j(\mathbf{x}_i) \tag{5.12}$$

The matrix Φ is a discrete version of the overlap matrix. The spatial and time derivatives of ϕ_i are simply calculated by taking the appropriate derivatives of Eq. (5.4). Since all calculations are run in the diabatic representation in this chapter, the derivative coupling terms are omitted for clarity. All coupling between the surfaces occurs through the off-diagonal elements of the potential energy, V^{IJ}.[9, 52, 58, 77]

Propagating independent trajectories leads to a highly unstructured grid that resembles the framework of the QTM. We demonstrate the collocation form of the trajectory-guided TDSE is capable of describing quantum mechanical processes while avoiding the rigidity of

a discrete variable representation grid and the numerical instabilities of the QTM.

Although Eq. (5.8) may be ill-conditioned, it can be readily solved for an accurate set of expansion coefficients $\{D_j^I\}$ through regularization methods for inverse problems.[78] We employ a singular value decomposition (SVD) with a threshold for removing small singular values. Similar regularization methods are employed for the Gaussian-based methods with Gaussian test functions.[29, 30, 79, 80]

5.3 Applications

5.3.1 Computational details

In all calculations the initial state is taken to be an N_d-dimensional Gaussian wave packet constructed as the product of one-dimensional Gaussians and populated on a single potential energy surface. The sinc pseudospectral method is used throughout as the reference.[36, 46–51, 81–84] In the reference calculations, the propagator is calculated by diagonalizing and exponentiating the Hamiltonian operator followed by repeated application of the propagator.

The width of the basis functions is set to the width of the initial state. The initial position and momenta were sampled from the appropriate Wigner distribution of a Gaussian wave function.[85, 86] The threshold to retain singular values was generally set to 1×10^{-4}. The equations were propagated using a fixed time step fourth-order Runge-Kutta algorithm. The initial expansion coefficients for time-dependent problems are determined by projecting the basis onto the initial wave function, $c(t=0) = \mathbf{\Phi}^{-1}\langle\delta(x-x_i)|\Psi\rangle$. The vector of elements $\langle\delta(x-x_i)|\Psi\rangle$, is the initial wave function evaluated at the basis function centers determined from sampling the Wigner distribution and $\mathbf{\Phi}^{-1}$ is the inverse of the discrete overlap matrix.

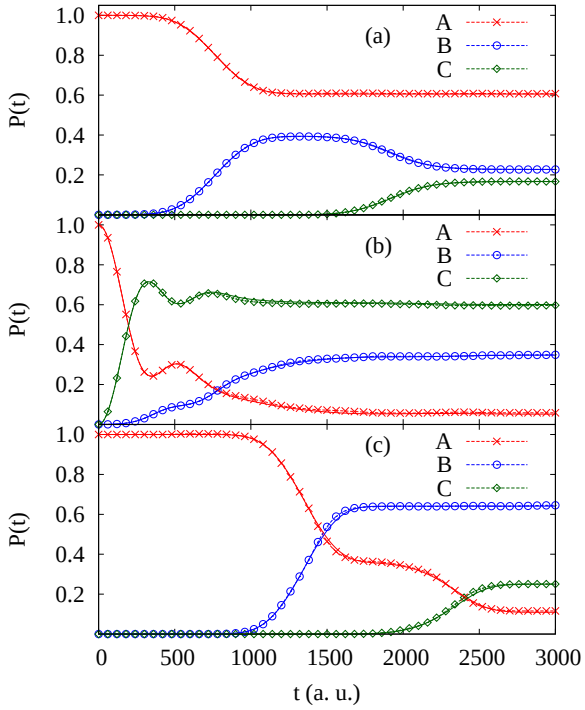

Figure 5.1: The time-dependent populations for three coupled surfaces in a prototypical photodissociation process. The initially occupied state (A) is denoted by x's, the second surface (B) by hollow circles, and the third (C) by hollow diamonds. The exact results are given by solid lines and nearly indistinguishable for all cases. All simulations used 150 trajectories.

5.3.2 Results

Morse potential

The first set of models investigated consist of Morse oscillator potential energy surfaces with Gaussian coupling between the surfaces. The coupled Morse potentials are a prototypical model for anharmonic vibrational dynamics and electron transfer.[69, 70, 87, 88] We will consider both dissociative and bound state conditions. The functional forms of the diabatic surfaces and coupling potentials are, respectively,

$$H_{ii}(x) = D_i \left(1 - e^{-a_i(x-b_i)}\right)^2 + E_i \tag{5.13}$$

$$H_{ij}(x) = A_{ij} e^{-c_{ij}(x-d_{ij})^2}. \tag{5.14}$$

First, we consider the photodissociation of a wave packet in a system of three coupled potential energy surfaces.[69, 88, 89] The original system parameters for the three cases may be found in Ref. [69]. The calculation is meant to model photodissociation following excitation from a harmonic ground state. The initial wave packet is taken to be high on the repulsive barrier, leading to dissociation after passage through the regions of nonadiabatic coupling. Given the qualitative similarity of the three Morse potentials, we can expect that Ehrenfest trajectories will appropriately cover important regions of phase space. Each simulation used 150 trajectories, a time step of 3 a.u., and an SVD threshold of 1×10^{-4}.

The time-dependent populations for the three states are presented in Fig. 5.1. In all three cases, 150 trajectories are sufficient to produce results indistinguishable from the exact calculation. In the first and third cases, the two regions of coupling are well-separated spatially while the second model couples all three surfaces in proximity. In all cases the pseudospectral Gaussian method correctly predicts the population exchange between all three surfaces. Since the pseudospectral Gaussian method solves the Schrödinger equation in matrix form, one might expect the proper treatment of the population transfer. We demonstrate that one may obtain accurate and efficient solutions by projecting the disordered Gaussian basis set onto discrete points in space.

A more challenging case is the bound state dynamics of two coupled Morse potentials A and B. In this model, the photo excitation results in a Gaussian wave packet starting on the shallow, attractive region of the initially occupied state, leading to oscillatory dynamics and many crossings through the region of nonadiabatic coupling. The parameters used in this chapter are $D_A = 2.278 \times 10^{-2}$, $a_A = 0.675$, $b_A = 1.89$, $E_A = 0.0$. $D_B = 1.025 \times 10^{-2}$, $a_B = 0.453$, $b_B = 3.212$, $E_B = 3.8 \times 10^{-3}$, $d_{AB} = 2.744$, $c_{AB} = 0.56$, $A_{AB} = 6.337 \times 10^{-3}$. They are slightly modified from the work of Coker and co-workers.[70, 88] The initial wave packet parameters are $x_c = 4.0$ a.u., $k_0 = 0.0$ a.u., mass= 2000.0 a.u. and $\alpha = 0.5$ a.u.$^{-2}$. The simulation is run for 10,000 a.u., approximately 240 femtoseconds, a time step of 5 a.u. and an SVD threshold of 1×10^{-2}.[88]

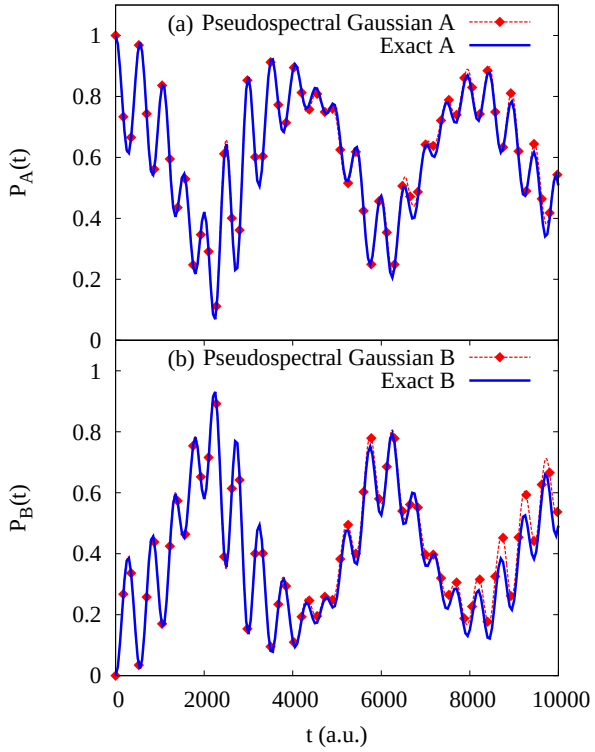

Figure 5.2: Time-dependent populations of the diabatic states for the bound state Morse model surface A (a) and B (b) using 1,000 trajectories. Both the high and low frequency oscillations corresponding to continuous nonadiabatic exchange and nuclear motion, respectively, are reproduced.

The time-dependent population dynamics using 1,000 trajectories are presented in Fig. 5.2. The bound state is characterized by two important time scales. First, there is the high frequency population exchange caused by continuous nonadiabatic transfer. There is also a slower oscillation in the populations corresponding to the nuclear wave packet motion. As a result, accurate population dynamics requires proper treatment of both inter- and intrastate coupling. The pseudospectral Gaussian method properly captures both of these effects, leading to quantitative agreement over the entire propagation. As a test of the quality of the intra-surface coupling, we plot the densities for the two surfaces at the final time in Fig. 5.3. The nodal features characteristic of the coherent dynamics are reproduced very well by the pseudospectral sampling.

While the results are well converged for 1,000 trajectories, we also present results using

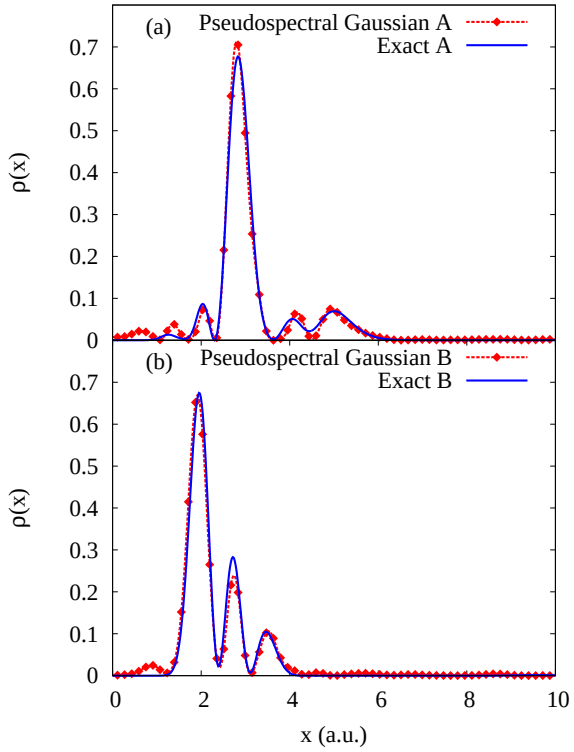

Figure 5.3: The density on surface A (a) and surface B (b) of the bound state Morse model at $t = 10,000$ a.u. using 1,000 trajectories. The pseudospectral Gaussian captures the nodal features in the density characteristic of coherent quantum dynamics in a Morse potential.

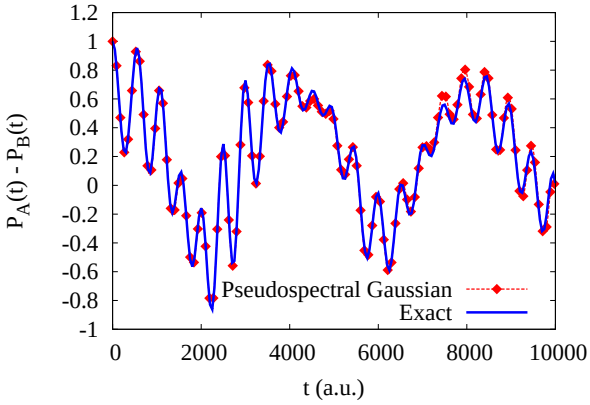

Figure 5.4: Time-dependent population difference of the diabatic surfaces for the bound state Morse potential using 250 trajectories. While the population differences quantitatively agree, calculating the population difference obscures the deviation in total norm. Nevertheless, the agreement is excellent.

250 trajectories. Fig. 5.4 plots the population difference, $P_A - P_B$, rather than the populations. The much smaller basis quantitatively describes the population exchange between

the two states. However, the total norm of the system at $t = 10,000$ is 1.23. The deviation in norm reflects the breakdown in the method as the basis set no longer sufficiently covers the important regions of phase space. Despite the accumulated error in the total norm, the pseudospectral Gaussian method still offers a quantitative description of the population exchange.

Two-Dimensional Conical Intersection

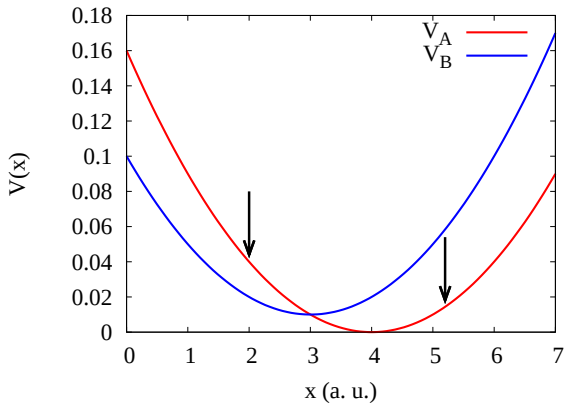

Figure 5.5: A cross section of the two-dimensional diabatic potentials along the x-axis at $y = 0$. The arrows mark the two initial wave packet positions. Both wave packets begin on V_A.

Finally, we investigate the nonadiabatic dynamics of a model for the vibrational dynamics of a collinear triatomic molecule ABA.[71, 72] The model describes the coupling between two electronic states with two degrees of freedom, the symmetric (x) and anti-symmetric (y) vibrational modes. The potential energy surfaces are

$$V_A(x,y) = \frac{1}{2}k_x(x-x_1)^2 + \frac{1}{2}k_y y^2$$

$$V_B(x,y) = \frac{1}{2}k_x(x-x_2)^2 + \frac{1}{2}k_y y^2 + \Delta \tag{5.15}$$

$$V_C(x,y) = \gamma y \exp\left(-\alpha(x-x_3)^2 - \beta y^2\right) \tag{5.16}$$

where $x_1 = 4$, $x_2 = x_3 = 3$, $k_x = 0.02$, $k_y = 0.1$, $\Delta = 0.01$, $\gamma = 0.01$, $\alpha = 3$ and

$\beta = 1.5$. The parameter γ controls the interstate coupling for the model. The initial wave packet is selected to model a Franck-Condon excitation from a harmonic ground state. The masses are $m_x = 20000, m_y = 6667$ a.u., the initial wave packet widths are $\alpha_x = 22.2$ and $\alpha_y = 12.9$ a.u.$^{-2}$, and the wave packet is centered at $y_0 = 0$ for both examples. In both cases $p_x = p_y = 0$

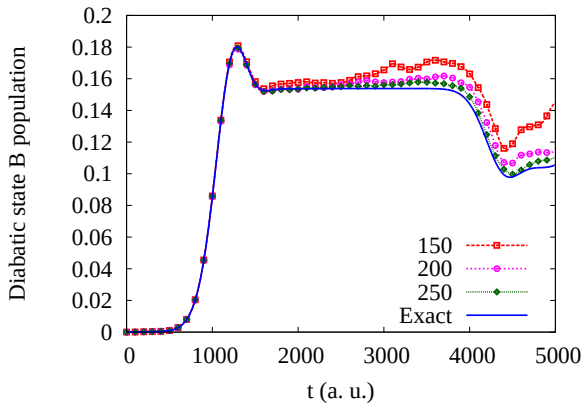

Figure 5.6: Time-dependent population for the upper diabatic surface for increasing basis set size and an initial wave packet centered at $(x, y) = (2, 0)$. The initial condition leads to a higher energy wave packet that completes the first passage through the region of nonadiabatic coupling at approximately 1,200 a.u. The three basis set sizes exhibit clear convergence to the exact solution with excellent agreement using 250 trajectories.

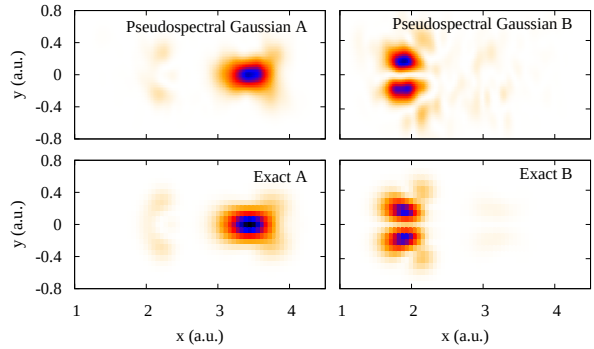

Figure 5.7: The wave packet densities at $t = 5,000$ a.u. from the wave packet starting at $(x, y) = (2, 0)$. The upper panels are the pseudospectral Gaussian method and the lower panels the exact grid calculation. There are patches of spurious density on the upper surface but otherwise all of the features are reproduced very well. Note the spatial separation of the density on the two surfaces.

First, we consider a wave packet starting at $x_0 = 2.0$ on surface A. As shown in Fig. 5.5,

the initial condition corresponds to an energy well above the crossing region. The wave packet was propagated for 5,000 a.u., capturing the initial passage through the coupling region and a second period where the density in the excited returns to the coupling region, leading to a small amount of population transfer back to the ground state. All basis set sizes predict the initial population transfer in excellent agreement with the exact method. However, as the simulation progresses, the smaller basis sets deteriorate in quality even when outside the region of nonadiabatic coupling. Inspection of the trajectories suggest the spurious population, accompanied by deviation of total norm, occurs when the Ehrenfest trajectories no longer cover the regions of density on the upper surface.

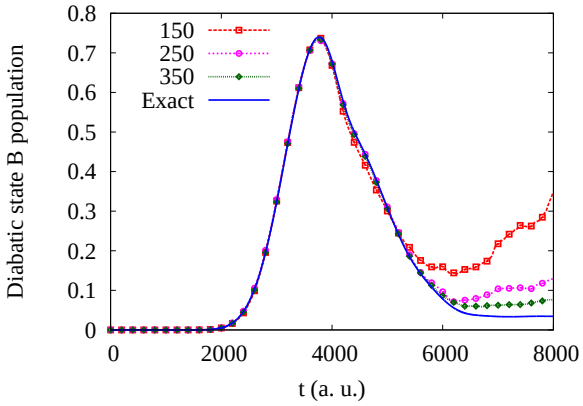

Figure 5.8: Time-dependent population for the upper diabatic surface for increasing basis set size and an initial wave packet centered at $(x, y) = (5.2, 0)$. The initial energy of the wave packet is approximately equal to the energy of the surface crossing resulting in many trajectories not reaching the crossing region. While there is significant population exchange upon reaching the crossing point, most of the density returns to the ground state following reflection off of the harmonic barrier. The smaller basis set predicts spurious population on the upper surface, particularly as the densities spatially separate and the Ehrenfest trajectories fail. The error is greatly reduced as basis set size increases.

The breakdown of Ehrenfest trajectories and the qualitative features of population transfer may be better understood by inspecting the densities on the respective surfaces at $t = 5,000$ a.u. in Fig. 5.7. Since the wave packet begins at $(x, y) = (2, 0)$, it first moves in the positive x-direction and passes through the region of derivative coupling, completing the initial population transfer in the first 1,500 time units. Now, a small portion of the

wave packet is propagating on the upper surface while most remains in the ground state. However, the classical turning point on surface B is at $x = 4.7$ but $x = 6$ on surface A. Therefore the momentum of the density on B changes sign earlier in time than A and passes through the region of derivative coupling again at 4,000 a.u. Since the wave packet is still predominantly on the lower surface, one would expect the trajectories to follow the forces of that surface. This, of course, prevents trajectories from following up the upper surface through the crossing at $t = 4,000$ a.u. The densities illustrate the spatial separation caused by the different forces.

The second crossing transfers some of the population from B back to A. This density is observable in both the approximate and exact calculations on surface A at $x = 2$, spatially separated from the principal wave packet density. The pseudospectral Gaussian method also reproduces the node in the upper surface that is a consequence of the Berry phase,.[90, 91] This phase relationship is only observable from a proper quantum mechanical treatment of the dynamics. While the qualitative failure of Ehrenfest trajectories is overcome by using larger basis sets, basis function spawning is a much more efficient solution and may be pursued in the future.

The densities on both surfaces at $t = 5,000$ a.u using 250 trajectories are plotted in Fig. 5.7. On surface A, the pseudospectral Gaussian method not only captures the majority of the wave packet at $x = 3.5$ but also the density at $x = 2$. The small population in this region is reflected by the loss of population on surface 2 at 4,000 a.u. in Fig. 5.6 that occurs when the wave packet density on surface B passes through the region of nonadiabatic coupling. The pseudospectral Gaussian method reproduces the node in the upper surface that is a consequence of the Berry phase.[90, 91]

In the second example, we begin with a wave packet centered at $x_0 = 5.2$, corresponding to lower energy dynamics. In this case, the wave packet reaches the crossing region with very little excess energy and many trajectories will not reach the intersection. As discussed in Yang *et al.* , this type of transition is very difficult for surface hopping methods.[72] The

time-dependent probability on the excited surface is plotted in Fig. 5.8. Similar to the first case, excellent agreement is observed for all basis set sizes for the first half of the propagation. At this time, the densities on the two states have considerably different momenta and the trajectories fail to follow the quantum mechanics. Interestingly, the pseudospectral Gaussian method converges to a final excited state population slightly above the exact result. While improved accuracy would be preferred, we note that the Gaussian based methods in Ref. [72] converge to a similar population.

5.4 Discussion

In this work, we introduce a Gaussian trajectory based approach to non-adiabatic dynamics that only requires $\mathcal{O}(N)$ potential energy calculations yet describes quantum mechanical coherence in the nuclear dynamics. Selecting the Dirac delta function, to test the Schrödinger equation, produces an efficient set of equations that circumvents the costly and inaccurate numerical integration of the potential energy generally associated with Gaussian basis sets with simple function evaluation. While traditional pseudospectral methods require highly structured grids, we demonstrate that accurate dynamics may still be realized despite abandoning a structured grid and basis function orthogonality.

The trajectory-guided basis of the pseudoGaussian method connects the method to many other trajectory based methods. Unlike surface hopping and semi-classical methods,[70, 77, 88, 92–101] quantum mechanics is incorporated explicitly by solving the Schrödinger equation in matrix form at each time step While the unstructured grid-like approach of pseudospectral Gaussian dynamics bears resemblance to Bohmian mechanics and the quantum trajectory method, the matrix formulation is fundamentally distinct from Bohmian mechanics and we suggest that it is more similar to pseudospectral methods.[102–107]

Effective dynamics using a trajectory-guided basis set relies on two components; efficient, local description of the quantum mechanics and coverage of important regions in phase space. In this work, we focus on the former, using the pseudo-Gaussian method to solve for the

quantum mechanics. The results in this chapter suggest that, when the basis set properly reflects the quantum mechanics, the pseudo-Gaussian method is very accurate. However, the Ehrenfest trajectories are suboptimal, particularly in the two-dimensional model presented here where the displacement of the surfaces lead to substantially different gradients for populations on the respective surfaces. Current interest lies in coupling the pseudospectral Gaussian method with a surface hopping or a spawning procedure, both of which improve upon the limitations of Ehrenfest trajectories.

Employing pseudospectral sampling offers a promising new approach to Gaussian based dynamics. The method adopts many of the attractive features of moving Gaussian basis sets while circumventing one of their greatest difficulties, the potential energy integral evaluation. We demonstrate that the pseudospectral Gaussian dynamics accurately describes both dissociative and bound state processes using a coupled Morse potential model and a model for collinear triatomic vibration. Using Ehrenfest guided trajectories, the method is able to simultaneously describe population dynamics and intra-surface dynamics for wave packets for long times. The successful implementation of the pseudospectral Gaussian method to one and two-dimensional nonadiabatic models suggests the method may be well-suited for *ab initio* on-the-fly non-adiabatic quantum molecular dynamics.

5.5 References

[1] D. R. Yarkony, J. Phys. Chem. **100**, 18612 (1996).

[2] L. J. Butler, Ann. Rev. Phys. Chem. **49**, 125 (1998).

[3] J. C. Tully, J. Chem. Phys. **137**, 22A301 (2012).

[4] M. Persico and G. Granucci, Theo. Chem. Acc. **133** (2014).

[5] I. Tavernelli, Acc. Chem. Res. **48**, 792 (2015).

[6] M. Ben-Nun and T. J. Martínez, Chem. Phys. Lett. **298**, 57 (1998).

[7] M. Ben-Nun and T. J. Martínez, J. Chem. Phys. **110**, 4134 (1999).

[8] M. Ben-Nun, J. Quenneville, and T. J. Martínez, J. Phys. Chem. A **104**, 5161 (2000).

[9] M. Ben-Nun and T. J. Martínez, Adv. Chem. Phys. **121**, 439 (2002).

[10] S. S. Iyengar and J. Jakowski, J. Chem. Phys. **122** (2005).

[11] B. Lasorne, M. J. Bearpark, M. A. Robb, and G. A. Worth, Chem. Phys. Lett. **432**, 604 (2006).

[12] B. Lasorne, M. A. Robb, and G. A. Worth, Phys. Chem. Chem. Phys. **9**, 3210 (2007).

[13] X. Li and S. S. Iyengar, J. Chem. Phys. **133**, 184105 (2010).

[14] K. Saita and D. V. Shalashilin, J. Chem. Phys. **137** (2012).

[15] C. Leveque, A. Komainda, R. Taieb, and H. Koppel, J. Chem. Phys. **138**, 044320 (2013).

[16] D. V. Makhov, W. J. Glover, T. J. Martínez, and D. V. Shalashilin, J. Chem. Phys. **141**, 054110 (2014).

[17] B. Lasorne, G. Worth, and M. Robb, in *Molecular Quantum Dynamics*, edited by F. Gatti (Springer Berlin Heidelberg, 2014), pp. 181–211.

[18] B. O. Roos, Acc. Chem. Res. **32**, 137 (1999).

[19] J. D. Coe, B. G. Levine, , and T. J. Martínez, J. Phys. Chem. A **111**, 11302 (2007).

[20] T. Tsuchimochi and G. E. Scuseria, J. Chem. Phys. **131**, 121102 (2009).

[21] H. Tao, B. G. Levine, and T. J. Martínez, J. Phys. Chem. A **113**, 13656 (2009).

[22] T. Yanai, Y. Kurashige, E. Neuscamman, and G. K.-L. Chan, J. Chem. Phys. **132**, 024105 (2010).

[23] D. A. Mazziotti, Chem. Rev. **112**, 244 (2012).

[24] D. Huber and E. J. Heller, J. Chem. Phys. **89**, 4752 (1988).

[25] T. J. Martínez, M. Ben-Nun, and R. D. Levine, J. Phys. Chem. **100**, 7884 (1996).

[26] D. V. Shalashilin and M. S. Child, J. Chem. Phys. **113**, 10028 (2000).

[27] L. Mauritz Andersson, The Journal of Chemical Physics **115**, 1158 (2001).

[28] Y. Wu and V. S. Batista, The Journal of Chemical Physics **118**, 6720 (2003).

[29] W. Koch and T. J. Frankcombe, Phys. Rev. Lett. **110**, 263202 (2013).

[30] M. A. C. Saller and S. Habershon, J. Chem. Theory Comput. **11**, 8 (2015).

[31] E. J. Heller, J. Chem. Phys. **62**, 1544 (1975).

[32] T. J. Martinez and R. D. Levine, J. Chem. Soc. Faraday T. **93**, 941 (1997).

[33] T. J. Martínez, M. Ben-Nun, and R. D. Levine, J. Phys. Chem. A **101**, 6389 (1997).

[34] G. A. Worth and I. Burghardt, Chem. Phys. Lett. **368**, 502 (2003).

[35] J. Boyd, *Chebyshev and Fourier Spectral Methods: Second Revised Edition*, Dover Books on Mathematics (Dover Publications, 2001).

[36] J. Lill, G. Parker, and J. Light, Chem. Phys. Lett. **89**, 483 (1982).

[37] D. Kosloff and R. Kosloff, J. Comput. Phys. **52**, 35 (1983).

[38] W. Yang and A. C. Peet, Chem. Phys. Lett. **153**, 98 (1988).

[39] R. Kosloff, J. Phys. Chem. **92**, 2087 (1988).

[40] A. C. Peet and W. Yang, J. Chem. Phys. **91**, 6598 (1989).

[41] A. C. Peet and W. Yang, J. Chem. Phys. **90**, 1746 (1989).

[42] W. Yang and A. C. Peet, J. Chem. Phys. **92**, 522 (1990).

[43] J. Sielk, H. F. von Horsten, F. Kruger, R. Schneider, and B. Hartke, Phys. Chem. Chem. Phys. **11**, 463 (2009).

[44] W. Yang, A. C. Peet, and W. H. Miller, J. Chem. Phys. **91**, 7537 (1989).

[45] M. Dehghan and A. Shokri, Comput. Math. Appl. **54**, 136 (2007).

[46] S. A. Orszag, Phys. Fluids **12**, 250 (1969).

[47] D. Gottlieb and S. Orszag, *Numerical Analysis of Spectral Methods: Theory and Applications* (SIAM, 1977).

[48] D. Furnaro, in *Polynomial Approximation of Differential Equations* (Springer-Verlag Heidelberg, 1992), vol. 8 of *Lecture Notes in Physics*.

[49] B. Fornberg, *A Practical Guide to Pseudospectral Methods* (Cambridge University Press, 1998).

[50] C. Canuto, M. Y. Hussaini, A. Quarteroni, and T. Zang, *Spectral Methods: Fundamentals in Single Domains* (Springer-Verlag Berlin Heidelberg, 2006).

[51] J. S. Hesthaven, S. Gottlieb, and D. Gottlieb, *Spectral methods for time-dependent problems* (Cambridge University Press, 2007).

[52] D. Tannor, *Introduction to Quantum Mechanics: A Time-dependent Perspective* (University Science Books, 2007).

[53] R. E. Wyatt, C. L. Lopreore, and G. Parlant, J. Chem. Phys. **114**, 5113 (2001).

[54] V. A. Rassolov and S. Garashchuk, Phys. Rev. A **71**, 032511 (2005).

[55] B. F. E. Curchod, I. Tavernelli, and U. Rothlisberger, Phys. Chem. Chem. Phys. **13**, 3231 (2011).

[56] N. Zamstein and D. J. Tannor, J. Chem. Phys. **137**, 22A517 (2012).

[57] N. Zamstein and D. J. Tannor, J. Chem. Phys. **137**, 22A518 (2012).

[58] B. F. E. Curchod and I. Tavernelli, J. Chem. Phys. **138**, 184112 (2013).

[59] E. R. Bittner and P. J. Rossky, J. Chem. Phys. **103**, 8130 (1995).

[60] G. Granucci, M. Persico, and A. Zoccante, J. Chem. Phys. **133** (2010).

[61] J. E. Subotnik, J. Chem. Phys. **132**, 134112 (2010).

[62] J. E. Subotnik and N. Shenvi, J. Chem. Phys. **134**, 024105 (2011).

[63] B. R. Landry and J. E. Subotnik, J. Chem. Phys. **135**, 191101 (2011).

[64] J. E. Subotnik, J. Phys. Chem. A **115**, 12083 (2011).

[65] N. Shenvi, J. E. Subotnik, and W. Yang, J. Chem. Phys. **135**, 024101 (2011).

[66] N. Shenvi, J. E. Subotnik, and W. Yang, J. Chem. Phys. **134**, 144102 (2011).

[67] J. E. Subotnik and N. Shenvi, J. Chem. Phys. **134**, 244114 (2011).

[68] B. R. Landry and J. E. Subotnik, J. Chem. Phys. **137**, 22A513 (2012).

[69] E. A. Coronado, J. Xing, and W. H. Miller, Chem. Phys. Lett. **349**, 521 (2001).

[70] S. Bonella and D. F. Coker, J. Chem. Phys. **118**, 4370 (2003).

[71] A. Ferretti, G. Granucci, A. Lami, M. Persico, and G. Villani, J. Chem. Phys. **104**, 5517 (1996).

[72] S. Yang, J. D. Coe, B. Kaduk, and T. J. Martínez, J. Chem. Phys. **130**, 134113 (2009).

[73] M. Born and K. Huang, *Dynamical Theory of Crystal Lattices*, International series of monographs on physics (Clarendon Press, 1998).

[74] E. J. Heller, J. Chem. Phys. **75**, 2923 (1981).

[75] G. D. Billing, Chemical Physics Letters **100**, 535 (1983).

[76] D. V. Shalashilin, J. Chem. Phys. **130**, 244101 (2009).

[77] J. C. Tully, Faraday Discuss. **110**, 407 (1998).

[78] P. Hansen, *Discrete Inverse Problems: Insight and Algorithms*, Fundamentals of Algorithms (SIAM, 2010).

[79] M. Ben-Nun and T. J. Martínez, J. Chem. Phys. **108**, 7244 (1998).

[80] I. Burghardt, M. Nest, and G. A. Worth, J. Chem. Phys. **119**, 5364 (2003).

[81] D. T. Colbert and W. H. Miller, J. Chem. Phys. **96**, 1982 (1992).

[82] J. C. Light and T. Carrington, Adv. Chem. Phys. **114** (2000).

[83] D. A. Mazziotti, Chem. Phys. Lett. **299**, 473 (1999).

[84] D. A. Mazziotti, J. Chem. Phys. **117**, 2455 (2002).

[85] E. Wigner, Phys. Rev. **40**, 749 (1932).

[86] E. J. Heller, J. Chem. Phys. **65**, 1289 (1976).

[87] S. Yeganeh and M. A. Ratner, J. Chem. Phys. **124**, 044108 (2006).

[88] P. Huo and D. F. Coker, Mol. Phys. **110**, 1035 (2012).

[89] J. R. Duke and N. Ananth, J. Phys. Chem. Lett. **6**, 4219 (2015).

[90] H. C. Longuet-Higgins, P. Roy. Soc. Lond. A Mat. **344**, 147 (1975).

[91] M. V. Berry, P. Roy. Soc. Lond. A Mat. **392**, 45 (1984).

[92] J. C. Tully, J. Chem. Phys. **93**, 1061 (1990).

[93] F. Webster, P. Rossky, and R. Friesner, Comput. Phys. Commun. **63**, 494 (1991).

[94] S. Hammes-Schiffer and J. C. Tully, J. Chem. Phys. **101**, 4657 (1994).

[95] O. V. Prezhdo and P. J. Rossky, J. Chem. Phys. **107**, 825 (1997).

[96] G. Stock and M. Thoss, Phys. Rev. Lett. **78**, 578 (1997).

[97] X. Sun and W. H. Miller, J. Chem. Phys. **106**, 6346 (1997).

[98] Y. Wu and M. F. Herman, J. Chem. Phys. **123**, 144106 (2005).

[99] W. H. Miller, J. Phys. Chem. A **113**, 1405 (2009).

[100] P. Huo and D. F. Coker, J. Chem. Phys. **135**, 201101 (2011).

[101] S. J. Cotton, K. Igumenshchev, and W. H. Miller, J. Chem. Phys. **141**, 084104 (2014).

[102] C. L. Lopreore and R. E. Wyatt, Phys. Rev. Lett. **82**, 5190 (1999).

[103] R. E. Wyatt and E. R. Bittner, J. Chem. Phys. **113**, 8898 (2000).

[104] R. E. Wyatt, D. J. Kouri, and D. K. Hoffman, J. Chem. Phys. **112**, 10730 (2000).

[105] X.-G. Hu, T.-S. Ho, H. Rabitz, and A. Askar, Phys. Rev. E **61**, 5967 (2000).

[106] B. K. Kendrick, J. Chem. Phys. **119**, 5805 (2003).

[107] R. Wyatt and C. Trahan, *Quantum Dynamics with Trajectories: Introduction to Quantum Hydrodynamics*, Interdisciplinary applied mathematics (Springer, 2006).

CHAPTER 6

CONCLUSION AND OUTLOOK

In this thesis, we introduce a new trajectory-based formulation for quantum molecular dynamics. Numerical studies of the time-dependent Schrödinger equation were pioneered by principles of exponentially convergent numerical methods. Spectral expansions, Gaussian quadrature, orthogonal polynomials and other ideas from numerical methods were explored to achieve numerically exact results. Simultaneously, the Gaussian wave packet was being popularized for approximate time propagation and semi-classical methods built a foundation for trajectory-based dynamics.

In the past thirty years, these two areas have grown considerably, offering a plethora of methods to study time-dependent quantum mechanics, including methods that bridge exact and semi-classical dynamics. It has become clear that trajectories are invaluable to chemically relevant studies. It is simply not feasible to construct a static grid in ten or twenty dimensions where the potential energy surface is unknown.

However, trajectories may refer to an independent point particle with a semi-classical amplitude or full variational coupled equations of motion for the basis set. If we wish to study meaningful chemistry, we must consider the electronic structure cost associated with the dynamics. Perhaps convergence is achieved with $\mathcal{O}(10^4)$ cheap, independent trajectories, or $\mathcal{O}(10^2)$ fully coupled trajectories that require solving a complicated system of equations at each step. If electronic structure calculations are required for the potential energy, the rate limiting step in the propagation may quickly become the electronic structure. This is a well-known concern but a fundamental consideration of the method development in this thesis.

We believe that grid methods are a promising avenue in developing methods capable of describing accurately and efficiently describing quantum dynamics. Traditionally, grids have been limited to pseudospectral methods with time-independent basis functions or Bohmian mechanics, both of which have been confined to relatively few dimensions. Nevertheless,

there has been significant interest recently in nontraditional grid methods.[1–5]

At this time, we have demonstrated that pseudospectral sampling of classically-guided Gaussian basis functions offers a compact and accurate description of quantum dynamics. The grid that we employ is similar, but distinct to both other grid methods and other Gaussian methods. As efforts to move forward in high-dimensional dynamics, the relationships between these methods need to be elucidated. We believe that the discretization of the wave function offers a unique perspective for method development capable of realizing new methods and unprecedented performance in quantum molecular dynamics.

6.1 References

[1] G. Hunter, Int. J. Quantum Chem. **9**, 237 (1975).

[2] I. Tavernelli, Phys. Rev. A **87**, 042501 (2013).

[3] G. Albareda, H. Appel, I. Franco, A. Abedi, and A. Rubio, Phys. Rev. Lett. **113**, 083003 (2014).

[4] G. Albareda, J. M. Bofill, I. Tavernelli, F. Huarte-Larrañaga, F. Illas, and A. Rubio, J. Phys. Chem. Lett. **6**, 1529 (2015).

[5] B. Gu and S. Garashchuk, J. Phys. Chem. A p. DOI: 10.1021/acs.jpca.5b10029 (2016).